



저작자표시-비영리-변경금지 2.0 대한민국

이용자는 아래의 조건을 따르는 경우에 한하여 자유롭게

- 이 저작물을 복제, 배포, 전송, 전시, 공연 및 방송할 수 있습니다.

다음과 같은 조건을 따라야 합니다:



저작자표시. 귀하는 원저작자를 표시하여야 합니다.



비영리. 귀하는 이 저작물을 영리 목적으로 이용할 수 없습니다.



변경금지. 귀하는 이 저작물을 개작, 변형 또는 가공할 수 없습니다.

- 귀하는, 이 저작물의 재이용이나 배포의 경우, 이 저작물에 적용된 이용허락조건을 명확하게 나타내어야 합니다.
- 저작권자로부터 별도의 허가를 받으면 이러한 조건들은 적용되지 않습니다.

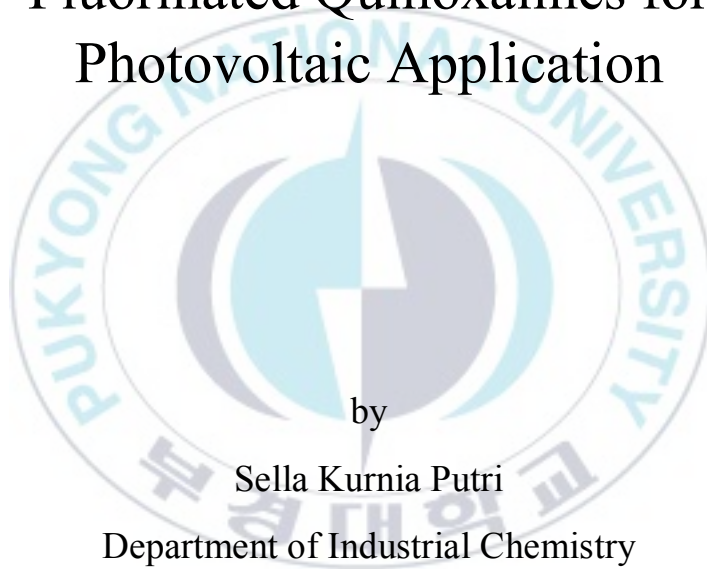
저작권법에 따른 이용자의 권리는 위의 내용에 의하여 영향을 받지 않습니다.

이것은 [이용허락규약\(Legal Code\)](#)을 이해하기 쉽게 요약한 것입니다.

[Disclaimer](#)

Thesis for the Degree of Master of Engineering

Synthesis and Characterization of  
Low Band-Gap Polymer based on  
Fluorinated Quinoxalines for  
Photovoltaic Application



by

Sella Kurnia Putri

Department of Industrial Chemistry

The Graduate School

Pukyong National University

August 25, 2017

# Synthesis and Characterization of Low Band-Gap Polymer based on Fluorinated Quinoxalines for Photovoltaic Application

Advisor: Dong Wook Chang

by

Sella Kurnia Putri

A thesis submitted in partial fulfillment of the requirements for the  
degree of

Master of Engineering

in Department of Industrial Chemistry, The Graduate School  
Pukyong National University

August, 2017

Synthesis and Characterization of Low Band-Gap  
Polymer based on Fluorinated Quinoxalines for  
Photovoltaic Application

A dissertation

by

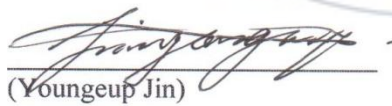
Sella Kurnia Putri

Approved by:



---

(Min Young Shon)



(Youngeup Jin)



---

(Dong Wook Chang)

August 25, 2017

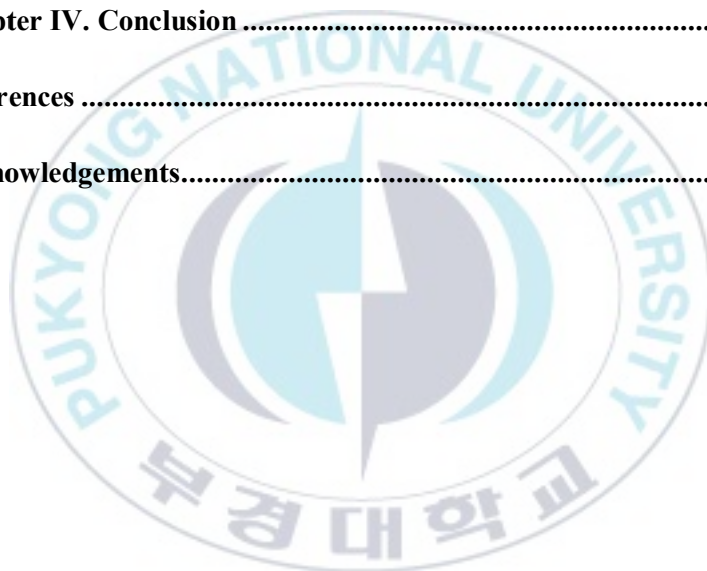
# Contents

Contents.....	i
List of Figures.....	v
List of Tables.....	viii
List of Schemes.....	ix
Abstract.....	x
<b>Chapter I. Introduction.....</b>	<b>1</b>
I-1. Polymer Solar Cells (PSCs).....	1
I-2. Basic Principles of PSCs.....	3
I-2.1. Photoexcitation and exciton formation.....	4
I-2.2. Exciton diffusion.....	4
I-2.3. Exciton dissociation.....	5
I-2.4. Charge transport and collection.....	5
I-3. Device Structure of PSCs.....	6
I-4. Parameter of PSCs.....	8
I-4.1. Open circuit voltage ( $V_{oc}$ ).....	9
I-4.2. Short Circuit Current Density ( $J_{sc}$ ).....	10
I-4.3. Fill Factor ( $FF$ ).....	10
I-4.4. Incident Photon to Current Efficiency (IPCE).....	11

I-5. Molecular Engineering Design of PSCs.....	1 2
I-5.1. Low band gap PSCs.....	1 2
I-5.2. Incorporation of fluorine atoms.....	1 4
I-5.3. Polymer backbone .....	1 5
I-5.3.1. Benzodithiophene as Donor backbone .....	1 5
I-5.3.2. Quinoxaline as Acceptor backbone.....	1 6
I-6. Aims of thesis .....	1 8
<b>Chapter II. Experimental Section.....</b>	<b>1 9</b>
II-1. Material and Instruments .....	1 9
II-2. Synthesis of Monomers.....	2 0
II-2.1. General Procedure for Stille Coupling Reaction.....	2 0
II-2.2. 4,7-Di(thiophen-2-yl)benzo[c][1,2,5]thiadiazole (3)	2 1
II-2.3. 5,6-Difluoro-4,7-di(thiophen-2-yl)benzo[c][1,2,5]thiadiazole (4).....	2 1
II-2.4. General Procedure for Acid-Catalyzed Reaction based on BT monomers .....	2 2
II-2.5. 2,3-Diphenyl-5,8-di(thiophen-2-yl)quinoxaline (7)	2 2
II-2.6. 2,3-Di(4-fluorophenyl)-5,8-di(thiophen-2-yl)quinoxaline (8) .....	2 3

II-2.7. 6,7-Difluoro-2,3-diphenyl-5,8-di(thiophen-2-yl)quinoxaline (9) .....	2 4
II-2.8. 6,7-Difluoro-2,3-bis(4-fluorophenyl)-5,8-di(thiophen-2-yl)quinoxaline (10) .....	2 4
II-2.9. General Procedure for Dibromination Reaction based on DPQ monomers .....	2 5
II-2.10. 5,8-Di(5-bromothiophen-2-yl)-2,3-diphenylquinoxaline (11) .....	2 5
II-2.11. 5,8-Di(5-bromothiophen-2-yl)-2,3-bis(4-fluorophenyl)quinoxaline (12).....	2 6
II-2.12. 5,8-Di(5-bromothiophen-2-yl)-6,7-difluoro-2,3-diphenylquinoxaline (13) .....	2 7
II-2.13. 5,8-Di(5-bromothiophen-2-yl)-6,7-difluoro-2,3-bis(4-fluorophenyl)quinoxaline (14).....	2 7
II-3. General Procedure for Polymerization by palladium-catalyzed Stille reaction .....	2 8
II-3.1. Synthesis of PBDT-Qx.....	2 8
II-3.2. Synthesis of PBDT-QxF .....	2 9
II-3.3. Synthesis of PBDT-FQx.....	2 9
II-3.4. Synthesis of PBDT-FQxF.....	3 0
II-4. Fabrication and analysis of photovoltaic devices .....	3 3

<b>Chapter III. Results and Discussion .....</b>	<b>3 5</b>
III-1. Synthesis and Thermal Properties of Polymers.....	3 5
III-2. Optical and Electrochemical Properties of Polymers .....	3 9
III-3. Theoretical Calculations of Polymers.....	4 6
III-4. Photovoltaic Properties of Polymers .....	4 9
<b>Chapter IV. Conclusion .....</b>	<b>5 7</b>
<b>References .....</b>	<b>5 8</b>
<b>Acknowledgements.....</b>	<b>6 2</b>



## List of Figures

- Figure I-1. Working mechanism of D-A heterojunction solar cell.
- Figure I-2. Chemical structures of electron-accepting fullerene derivatives PC<sub>61</sub>BM and PC<sub>71</sub>BM.
- Figure I-3. Conventional device (*left*) and inverted device (*right*) structure
- Figure I-4. J-V curves of PSCs in the dark and under illumination.
- Figure I-5. Molecular orbital of D-A type polymer leading to low band gap PSCs.
- Figure I-6. Benzodithiophene units with different substitutions.
- Figure I-7. Quinoxaline unit
- Figure II-1. Chemical structures of **PBDT-QxF**, **PBDT-QxF**, **PBDT-FQx**, and **PBDT-FQxF**.
- Figure III-1. TGA thermograms of **PBDT-Qx**, **PBDT-QxF**, **PBDT-FQx** and **PBDT-FQxF** at a heating rate of 10 °C/min under N<sub>2</sub>.
- Figure III-2. First cooling and second heating DSC thermograms of polymers with cooling and heating rate of 10 °C/min under N<sub>2</sub>:  
(a) **PBDT-QX**; (b) **PBDT-QxF**; (c) **PBDT-FQx**; (d) **PBDT-FQxF**.

Figure III-3. (a) UV-visible spectra of polymer films on a glass substrate (film spectra are offset for clarity) and (b) in chlorobenzene.

Figure III-4. Cyclic voltammograms of polymers.

Figure III-5. Energy level diagrams of polymers and materials in this research.

Figure III-6. Optimized geometries of the two repeating unit models of the DPQ-based polymers with a syn- and anti- configuration obtained by DFT calculation.

Figure III-7. Frontier molecular orbitals of two-repeating unit models with HOMO/LUMO energy levels calculated at the B3LYP/6-31G\*\* level for (a) **PBDT-Qx**, (b) **PBDT-QxF**, (c) **PBDT-FQx**, and (d) **PBDT-FQxF**.

Figure III-8. (a) Current density vs. voltage curves of PSCs under 1.0 sun condition (inset: under the dark condition) and (b) IPCE spectra of PSCs based on **PBDT-Qx** (square), **PBDT-QxF** (circle), **PBDT-FQx** (triangle) and **PBDT-FQxF** (inverted triangle).

Figure III-9. Current density vs. voltage curves of (a) electron- and (b) hole-only devices (inset: current density vs. voltage - built-in voltage ( $V_{bi}$ ) curves with fitted lines) based on **PBDT-Qx** (square), **PBDT-QxF** (circle), **PBDT-FQx** (triangle) and **PBDT-FQxF** (inverted triangle).

Figure III-10. AFM images of the active layers based on (a) **PBDT-Q<sub>x</sub>**,  
(b) **PBDT-Q<sub>x</sub>F**, (c) **PBDT-FQ<sub>x</sub>**, and (d) **PBDT-FQ<sub>x</sub>F**.

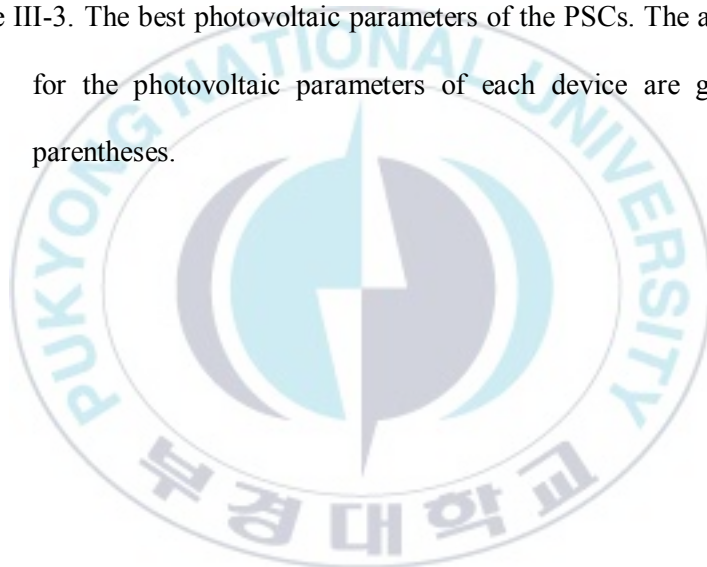


## List of Tables

Table III-1. Molecular weights of polymers.

Table III-2. Summary of optical and electrochemical properties of the polymers.

Table III-3. The best photovoltaic parameters of the PSCs. The averages for the photovoltaic parameters of each device are given in parentheses.



## List of Schemes

Scheme 1. Synthetic route of monomers and polymers.



Synthesis and Characterization of Low Band-Gap Polymer based on Fluorinated  
Quinoxalines for Photovoltaic Application

Sella Kurnia Putri

Department of Industrial Chemistry, The Graduate School,  
Pukyong National University

**Abstract**

A series of low-band gap fluorinated quinoxaline based donor- $\pi$ -acceptor conjugated polymer of **PBDT-Q<sub>x</sub>**, **PBDT-Q<sub>x</sub>F**, **PBDT-FQ<sub>x</sub>**, and **PBDT-FQ<sub>x</sub>F**, have been successfully synthesized via Stille coupling reaction. The polymers composed by electron-donating dialkoxy-substituted benzodithiophene (BDT) and electron-withdrawing 2,3-diphenylquinoxaline (DPQ) through a thiophene bridge. To understand the impact of fluorine (F) as strong electron-withdrawing moieties, the polymers have been substituted by F atoms in various number and at divers positions on the DPQ units such as the 6,7-positions, the para-positions of the phenyl substituent on the 2,3-positions, and both locations, and compared to non-fluorinated counterpart. Overall performances present a gradual enhancement of power conversion efficiencies (PCEs) due to favorable effect of F atoms. An optimize

device of inverted-type polymer solar cells (PSCs) with structure of ITO/ZnO/polymers:PC<sub>71</sub>BM/MoO<sub>3</sub>/Al showed that PBDT-FQxF, with four fluorine atoms on the 6,7-positions and the para-positions of the phenyl substituent on 2,3-positions of DPQ, exhibits the highest PCE of 6.60% with an open-circuit voltage ( $V_{oc}$ ) of 0.91 V, a short-circuit current density ( $J_{sc}$ ) of 10.15 mA/cm<sup>2</sup>, and a fill factor ( $FF$ ) of 71.50%.



# **Chapter I. Introduction**

## **I-1. Polymer Solar Cells (PSCs)**

Energy is one of essential matter in life, without energy, people may have many difficulties to live. Major world energy sources that are being used today are fossil energy (coal, natural gas, and oil) which is non-renewable source energy type and nowadays there over consumption that can lead to a serious environmental issues and world deficiency energy. In order to overcome above issues, advanced countries and scientists have been finding and developing alternative renewable energies such as bioenergy, wind power, hydro power, geothermal energy and solar energy. Solar energy became the most promising and efficient technologies to meet the worlds large and growing energy demand due to its abundance and cleanest energy. Solar cells convert the energy from sunlight directly into electricity by photovoltaic effect. Recently, inorganic solar cell based on materials, mainly crystalline silicon which is available commercially, take the most photovoltaic (PV) market and exhibit relative high power conversion efficiency (PCE) around 15-20%. However, the high cost of materials and its manufactured have been hindering its development. To search preferable solar cell technology, scientific research has been explored a polymer solar cell (PSCs) which

have low-cost material, light-weight, mechanical flexibility, easy processability and large-scale production. Presently, bulk-heterojunction (BHJ) device is known as the most efficient type of PSCs which donor (D) and acceptor (A) materials are blends together to form a bicontinuous interpenetrating network with large interfacial areas to afford efficient exciton dissociation [1]. Over past two decades of endeavors to discovered and improved a good materials and process techniques for device optimization, performance of PSCs have been driven to a high PCE over 10% [2-4]. Extensive research effort tries to develop a high-performance PSCs by designed and synthesized of new  $\pi$ -conjugated organic semiconductor.

## I-2. Basic Principles of PSCs

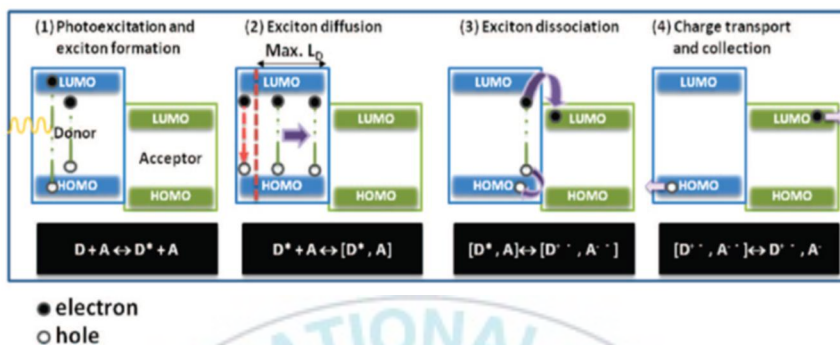


**Figure I-1.** Working mechanism of D-A heterojunction solar cell

Figure I-1 showed operating fundamental principle of PSCs which explain in four steps [5]. First, when sunlight absorbed into active layer form an exciton. Second, exciton diffusing to the interface between donor and acceptor. Third, exciton dissociates via an electron-transfer process. Fourth, separated free charge carriers (holes and electrons) were collected at anode and cathode, respectively.

### **I-2.1. Photoexcitation and exciton formation**

The presence of conjugated pi-electron system in organic compounds results in all interesting optical and electrical properties. The bandgap or bond energy in organic semiconductors is tuned with the energy of solar spectrum causing the absorption of photons producing electrostatically coupled electron-hole pairs called excitons. In case of inorganic silicon semiconductors, produces free charges instead of excitons. This major change drives all the differences in mechanism of electricity generation in inorganic and organic solar photovoltaic devices.

### **I-2.2. Exciton diffusion**

The photo generated excitons are characterized by very small lifetime of few picoseconds limiting the mobility of excitons to a few polymer units or molecules. The exciton moves within the chain causing chain deformation in order to reduce the extra unstable energy, which is altogether called polaron. However inter-molecular transition of excitons also happens which is termed as hopping process. Altogether the overall mobility of excitons are limited to a range of 10 nm, which is called the exciton diffusion length. As the excitons are to be dissociated within the

range of this length, exciton diffusion length plays a critical role in design and performance of organic solar cells.

### **I-2.3. Exciton dissociation**

Exciton dissociation refers to the process of splitting the electrostatically coupled electron-hole pair into free charges. The dissociation of excitons occurs at the donor-acceptor interfaces or junctions. The donor and acceptor materials are designed such that there exists a difference in LUMO levels of the materials, which drives the exciton dissociation. For efficient dissociation, the difference in energy level of LUMO of donor and acceptor should be higher than that of exciton binding energy. Typically the difference is around 0.2-0.3 eV.

In general, to achieve efficient charge separation

$$\Delta (LUMO_D - LUMO_A) > \text{Exciton binding energy}$$

### **I-2.4. Charge transport and collection**

Once the free charges are produced, they travel through specific materials to get collected at the electrodes. From there they are connected to the external circuit. The efficiency of charge transport are

determined by the electrical conductivity and impedance of the organic materials [6-9].

### **I-3. Device Structure of PSCs**

Bulk heterojunction (BHJ) PSCs is known as one of most promising method to fabricated photovoltaic device. Sandwich structure is the simplest structure of BHJ-PSCs which blending conjugated (donor) and fullerene derivative (acceptor) such as [6,6]-phenyl C<sub>61</sub> butyric acid methyl ester (PC<sub>61</sub>BM) or [6,6]-phenyl C<sub>71</sub> butyric acid methyl ester (PC<sub>71</sub>BM) (Fig. I-2) was sandwiched between a transparent metal oxide (indium tin oxide (ITO) and metal electrode) [10]. In conventional device structure, ITO and low work-function (Li, Ca and Al) metal are used as anode and cathode, respectively. Meanwhile, in an inverted device structure, the modified ITO and high work-function metal (Au, Ag and Cu) are cathode and anode, respectively. The differences between those structures showed in Figure I-3. Compared to the conventional device, high work-function used in inverted device are chemical resistance to oxygen and moisture, optical transparency and facile solution processability than low work-function metal which may be easily oxidized in the ambient environment which allows the diffusion of oxygen into active layer causes device degradation.

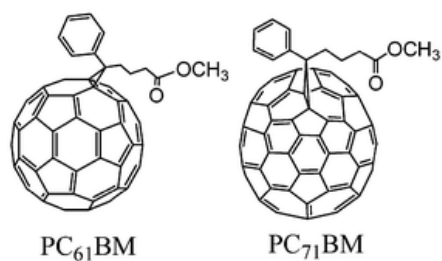


**Figure I-2.** Chemical structures of electron-accepting fullerene derivatives  $PC_{61}BM$  and  $PC_{71}BM$

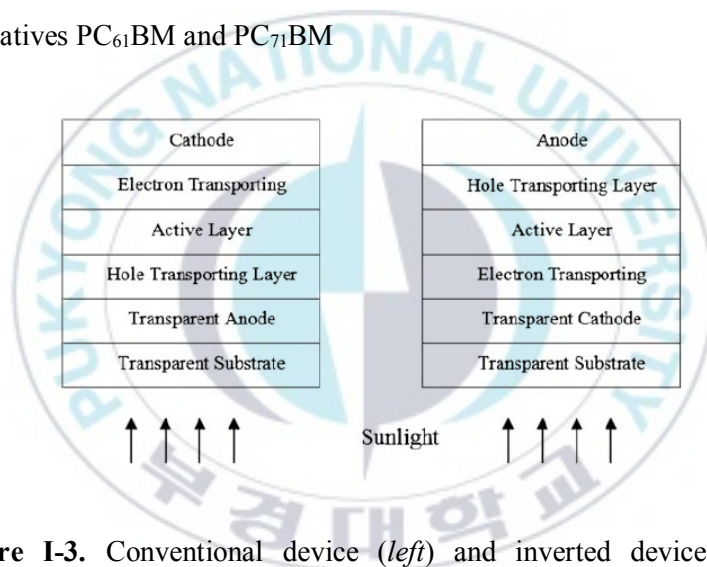


**Figure I-3.** Conventional device (*left*) and inverted device (*right*) structure

#### I-4. Parameter of PSCs

Parameter of photovoltaic performance PSCs calculated based on PCE which determined by the following formula:

$$PCE = \frac{V_{oc} \times J_{sc} \times FF}{P_{in}}$$

( $P_{in}$  is the incident light power density)

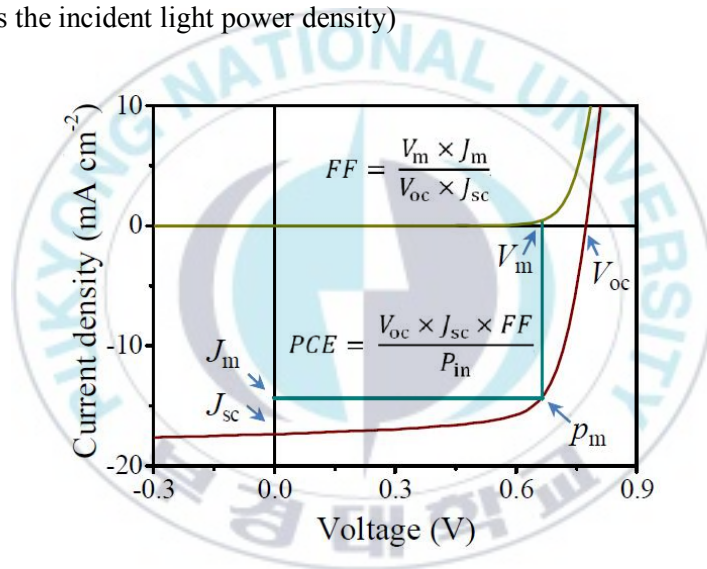


**Figure I-4.** J-V curves of PSCs in the dark and under illumination [11]

#### **I-4.1. Open circuit voltage ( $V_{oc}$ )**

The open circuit voltage ( $V_{oc}$ ) is the maximum voltage at which no current flows through the external circuit. Studies have demonstrated that  $V_{oc}$  is correlated to energy difference between the highest occupied molecular orbital (HOMO) level of donor polymer and the lowest unoccupied molecular orbital (LUMO) level of acceptor (mostly fullerene derivatives) at D-A interface of BHJ device. Based on this explanation, it can be noted that designing the conjugated polymer that match well with energy level of acceptor (mostly PCBM) are substantial. Because of PCBM have deep HOMO level, it necessary to adjusted also deep HOMO level of conjugated polymer to afford better charge-separation and transport characteristics which lead to higher  $V_{oc}$  [12], but overly deep HOMO level contrarily will enlarge band gap of the polymer which can driving to less photon absorbance. This is became main issue to design polymer with deep HOMO level PSCs but it have low band-gap level.

### **I-4.2. Short Circuit Current Density ( $J_{sc}$ )**

The short-circuit current density ( $J_{sc}$ ) is the current that flows through when the electrodes of the solar cell are short circuited. The  $J_{sc}$  is used to describe the maximum current delivered by a solar cell. The  $J_{sc}$  of a solar cell depends on the photon flux incident on the solar cell, which is determined by the spectrum of the incident light. For standard solar cell measurements, the spectrum is standardized to the AM1.5 spectrum. Most of the solar energy is concentrated in the visible and near-infrared (near-IR) region, to achieve high  $J_{sc}$ , polymer should have a large overlap with the solar spectrum in this region [1].

### **I-4.3. Fill Factor ( $FF$ )**

The fill factor ( $FF$ ) is the ratio between the maximum power generated by a solar cell and the product of  $V_{oc}$  with  $J_{sc}$ . The  $FF$  can give information about all of processes including the charge recombination, transport and collection. Also, the film morphology has direct effect of  $FF$  measurement. The  $FF$  defines the shape of the J-V curve, the ideal value of  $FF$  is unity (100%), when the J-V curve is a rectangle which defined as

$$FF = \frac{J_m \times V_m}{V_{oc} \times J_{sc}}$$

Where  $J_m$  and  $V_m$  are the current density and the voltage at the point of maximum output power, respectively (Fig I-3).

#### I-4.4. Incident Photon to Current Efficiency (IPCE)

Incident photon to current efficiency (IPCE), also known as External Quantum Efficiency (EQE) measurement is the ratio between the number of collected carriers ( $N_e$ ) and the number of all incident photons ( $N_p$ ) on the active area of the device as a function of wavelength. The IPCE measurement can describe how much of the absorbed photons are converted to current which determined by measurement of short-circuit current  $J_{sc}$  and the incident light intensity  $J_0$  as a function of the wavelength.

$$IPCE = \frac{N_e}{N_p} = \frac{J_0/e}{P_0 / \left(\frac{hc}{\lambda}\right)} = \frac{J_0 \times h \times c}{P_0 \times e \times \lambda}$$

where  $h$  is the Plank's constant,  $c$  is the speed of light,  $e$  is the electron charge,  $\lambda$  is the wavelength of the monochromatic light

$$IPCE = 1240 \frac{J_0}{P_0 \times \lambda}$$

where  $J_0$  is in the unit of  $\text{mA}/\text{cm}^2$ ,  $P_0$  is in the unit of  $\text{mW}/\text{cm}^2$ ,  $\lambda$  is in the unit of nm.

Ideally, the IPCE should equal to 100% across the entire wavelength range. However, in practice the effect of charge recombination limits the IPCE.

## **I-5. Molecular Engineering Design of PSCs**

As mentioned before, to produce high-performance BHJ device, we have to design PSCs (donor) which have well match energy level with fullerene derivatives (acceptor). Moreover, an ideal PSCs should have convenient energy levels, broad absorption ability and high charge carrier mobilities. Several strategies have been studied to aim this ideal PSCs:

### **I-5.1. Low band gap PSCs**

Recently, an important invention in design PSCs is used D-A type, which extensively develops most for donor material in BHJ device. This type composed by electron rich (D) unit and electron deficient (A) moiety within the fundamental repeating unit so that energy level and molecular structures can be optimized leading to narrow band gap to better harvest the solar spectrum with deep HOMO level and higher  $V_{oc}$

(Fig. I-5). Great effort in the research has been devoted to produce a low band gap (LBG) PSCs which typically have a band gap below 2 eV and absorption near infrared region longer than 620 nm thus enhanced the short-circuit current density ( $J_{sc}$ ) resulting in high PCE. Furthermore, LBG has more delocalized  $\pi$  electrons, extended conjugation and improving the planarity compared to wide band gap (WBG) counterparts [13, 14]. The most straightforward way to reduce the band gap is simply by either raising the HOMO or lowering the LUMO level of the PSCs or by compressing the two levels closer together simultaneously. But, the raising HOMO will decrease the  $V_{oc}$  value.

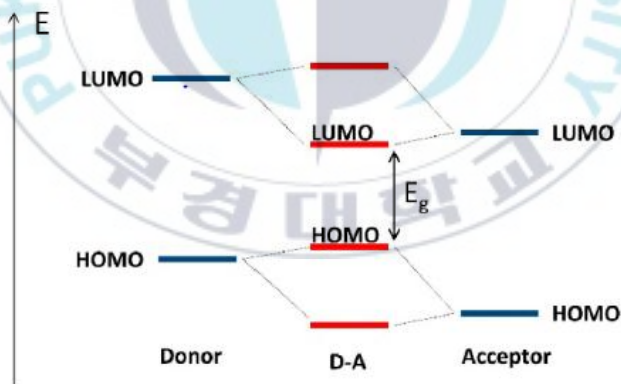


**Figure I-5.** Molecular orbital of D-A type polymer leading to low band gap PSCs.

## I-5.2. Incorporation of fluorine atoms

The big advantages of D-A type compared to early stage development donor poly(3-hexylthiophene) (P3HT) is its ease to modify the PSCs structures due to many more spot along the backbone and side chains to incorporate with functional atoms such as fluorine, and cyano group. Recent studies has great attention to introducing fluorine atoms in PSCs due to its unique features: (1) fluorine atom as electron-withdrawing has small van der Waals radius (1.35 Å) than hydrogen (1.2 Å); (2) fluorine atom compare to hydrogen has stronger electronegative element with a Pauling electronegativity of 4.0 than hydrogen only 2.2 [15-17]. Regarding to enhance PCE performance, fluorination can lowering both LUMO and HOMO energy level without increasing unexpected steric hindrance effect [11]. Deep HOMO level can promote  $V_{oc}$  resulting in higher PCE compare to non-fluorinated. Moreover, fluorination can impact to both inter- and intramolecular interaction such as C-F $\cdots$ H, F $\cdots$ S, C-F $\cdots$  $\pi_F$  to improve the crystallinity of polymer lead to higher planarity [15, 18]. As a result, polymer has good morphology and higher carrier mobility giving an improvement of  $J_{sc}$ ,  $FF$  and PCE [13, 18, 19-22].

### **I-5.3. Polymer backbone**

The backbone of PSCs refer to conjugation system has essential responsible to determine the optoelectronic properties of its PSCs such as band gap, energy level, charge carrier mobility and conductivity. Over past decade, research interest put their effort to develop various backbones. Several donor-acceptor PSCs with the its combination has been introduced such as 2,1,3 benzothiadiazole (BT), quinoxaline (Qx), diketo-pyrrolo-pyrrole (DPP), thienopyrroledione (TPD), dithienosilole (DTS), indacenodithiophene (IDT), benzo[1,2-b:4,5-b']dithiophene (BDT).

#### **I-5.3.1. Benzodithiophene as Donor backbone**

Benzo[1,2-b:4,5-b']dithiophene (BDT) unit (Fig. I-6) became one of the most successful unit to synthesize highly efficient PSCs due to rigid fused aromatic system which can enhance the electron delocalized and interchain  $\pi$ - $\pi$  interaction to improve high hole mobilities. Therefore, its planar conjugated structure resulting in convenient and highly tunable molecular energy levels and optical band gaps. BDT as a medium electron donating unit will contribute to low HOMO level which ensure

a high  $V_{oc}$  and its combination with strong acceptor can afford varieties of high-performance PSCs [23].

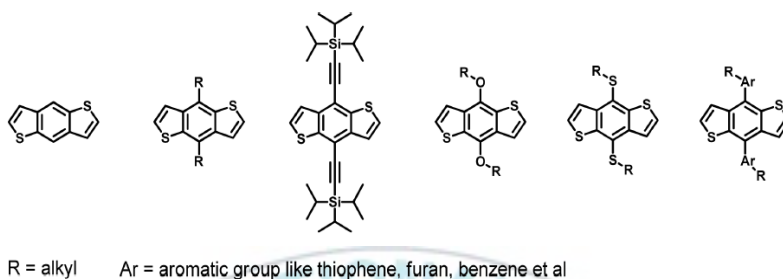


**Figure I-6.** Benzodithiophene units with different substitutions.

### I-5.3.2. Quinoxaline as Acceptor backbone

Due to its two nitrogen atoms as strong electronegative and two fused six-member rings, quinoxaline (Qx) (Fig. I-7) has unique characteristics. In this past few years, its derivatives have been extensively employed in wide applications such as organic light-emitting diodes (OLEDs), in dyes, efficient electroluminescent materials [24]. Chang and coworkers have demonstrated important invention in Qx, formation of vertical (2,3-diphenyl rings on Qx units) and horizontal (5-position of the Qx unit) of an electron donor which aim to tuning optoelectronic properties and controllable molecular structures [25]. Moreover, combination of Qx with various donor units such as indacenodithiophene (IDT),

dithienosilole (DTS), benzothiadiazole (BT), and benzodithiophene (BDT), *etc*, which D-A copolymers based Qx have been developed.

Qx is typically building block which can easily modified by attaching various side chains, such as alkyl chains, aromatic rings, functional group, *etc* which can afford different optoelectronic polymers.

Advantages of Qx is that it can attached by alkyl to enhance the solubility of conjugated polymers without presenting significant steric hindrance effect. Furthermore, by introduced side chain to the periphery Qx can provide more convenient controllable energy level, absorption, and morphology which can lead to high PCE. Kitazawa et al reported the introduction of various types of substituents at the 2,3-positions of Qx, demonstrated that by introduced side chain to the periphery Qx at these positions gave rise to the lower energy bandgap of the copolymer [26].

In addition, introduction of functional group or backbone modulation on the conjugated backbone Qx have been found can improve charge mobility of active layers, morphology and molecular packing performance, thus enhancing  $J_{sc}$  and  $FF$  values [27].

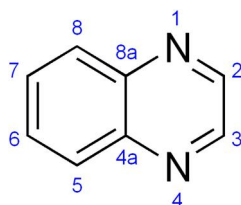


**Figure I-7.** Quinoxaline unit

### **I-6. Aims of thesis**

The aims of this thesis is to synthesized a series of electron-accepting 2,3-diphenylquinoxaline (DPQ) and electron donating dialkoxy-substituted benzodithiophene (BDT)-based low-band-gap polymers with a typical D- $\pi$ -A configuration. For systematic investigations, fluorine atoms were incorporated onto the 6,7-positions of DPQ, the para-positions of the phenyl substituents on the 2,3-positions of DPQ and both locations on the DPQ unit and compared to a non-fluorinated DPQ as a standard polymer.

## Chapter II. Experimental Section

### II-1. Material and Instruments

2,6-bis(trimethyltin)-4,8-bis(2-octyldodecyloxy)benzo[1,2-*b*:4,5-*b'*]dithiophene (**15**) used as donor monomer were synthesized according to the previous literatures [28]. Benzil and 4,4'-difluorobenzil were purchased from Aldrich and TCI, respectively. All other reagent and solvents were purchased from Aldrich Chemical Co., Inc.  $^1\text{H}$ ,  $^{13}\text{C}$ , and  $^{19}\text{F}$  NMR spectra were measured with a JEOL JNM ECP-400 spectrometer. UV-visible spectra were recorded on a JASCO V-530 UV-Vis spectrophotometer. Matrix-assisted laser desorption/ionization time-of-flight (MALDI-TOF) spectroscopy was conducted by using a Bruker Ultraflex spectrometer. Gel permeation chromatography (GPC) was measured on an Agilent 1200 series instrument with THF as the eluent. Cyclic voltammetry (CV) measurements were carried out by using a VersaSTAT3 potentiostat (Princeton Applied Research) with tetrabutylammonium hexafluorophosphate (0.1 M,  $\text{Bu}_4\text{NPF}_6$ ) as the electrolyte in acetonitrile. For CV measurements, a glassy carbon electrode coated with polymers and a platinum wire were used as the working and counter electrode, respectively. A silver wire was used as a pseudo-reference electrode with a ferrocene/ferrocenium external

standard. The thickness of the films was measured with an Alpha-Step IQ surface profiler (KLA-Tencor Co.), and the atomic force microscopy (AFM) topography images were taken by using a Bruker (NanoScope V) microscope operated in tapping mode.

## **II-2. Synthesis of Monomers**

### **II-2.1. General Procedure for Stille Coupling Reaction**

A mixture of dibromobenzothiadiazole (**1** or **2**, 3.4 mmol), 2-(tributylstannyl)thiophene (2.2 equiv., 5.9 mmol) and bis(triphenylphosphine)palladium(II) dichloride ( $\text{Pd}(\text{PPh}_3)_2\text{Cl}_2$ ) (3 mol% equiv., 0.068 mmol) were dissolved in dry tetrahydrofuran (THF) (15 ml). After  $\text{N}_2$  had been bubbled through for 15 min, the reaction mixture was heated at 60 °C and stirred for 12 hr under a  $\text{N}_2$  atmosphere. Upon completion of the reaction, the solution was cooled to room temperature and filtered with celite to remove the palladium catalyst. Solvents were removed under reduced pressure, and the crude residue was further purified by recrystallization with ethanol.

### II-2.2. 4,7-Di(thiophen-2-yl)benzo[c][1,2,5]thiadiazole (3)

Synthesis of compound **3** was followed by the general procedure for the Stille Coupling reaction. 4,7-dibromobenzo[c][1,2,5]thiadiazole (**1**) and 2-(tributylstannyl)thiophene were used as reactants. Yield: 88% (red solid needle). <sup>1</sup>H NMR (400 MHz, CDCl<sub>3</sub>): δ (ppm) = 8.11 (d, 2H, *J* = 8.5 Hz), 7.87 (s, 2H), 7.46 (d, 2H, *J* = 5.0 Hz), 7.21 (m, 2H). <sup>13</sup>C NMR (100 MHz, CDCl<sub>3</sub>): δ (ppm) 126.1, 126.4, 127.2, 127.9, 128.4, 139.7, 153.0.

### II-2.3. 5,6-Difluoro-4,7-di(thiophen-2-yl)benzo[c][1,2,5]thiadiazole (4)

Synthesis of compound **4** was followed by the general procedure for the Stille Coupling reaction. 5,6-difluoro-4,7-di(thiophen-2-yl)benzo[c][1,2,5]thiadiazole (**2**) and 2-(tributylstannyl)thiophene were used as reactants. Yield: 78% (dark red solid needle). <sup>1</sup>H NMR (400 MHz, CDCl<sub>3</sub>): δ (ppm) = 8.30 (d, 2H, *J* = 3.3 Hz), 7.62 (dd, 2H, *J* = 5.1, 0.9 Hz), 7.27 (t, 2H, *J* = 4.5 Hz). <sup>13</sup>C NMR (100 MHz, CDCl<sub>3</sub>): δ (ppm) = 111.0, 127.5, 129.0, 131.0, 131.6, 148.8, 149.0, 151.0.

## II-2.4. General Procedure for Acid-Catalyzed Reaction based on BT monomers

A mixture of the appropriate thiophene-attached benzothiadiazoles (**3** or **4**, 2.5 mmol) and zinc powder (20 equiv., 50 mmol) in acetic acid (60 mL) was stirred at 80 °C for 12 h. Upon completion of the reaction, the mixture was filtered to remove zinc powder and the filtrate was carefully collected. After addition of  $\alpha$ -diketone (benzil or 4,4'-difluorobenzil, 2.5 mmol) to the filtrate, the solution was heated to reflux overnight. The solution was cooled to room temperature, and the mixture was poured into water and extracted with chloroform. The organic layers were separated, dried over magnesium sulfate, and filtered. Solvents were removed under reduced pressure, and the crude residue was further purified by column chromatography with chloroform/ethanol (1/4, v/v).

## II-2.5. 2,3-Diphenyl-5,8-di(thiophen-2-yl)quinoxaline (**7**)

Synthesis of compound **7** was followed by the general procedure for the acid-catalyzed reaction. 4,7-Di(thiophene-2-yl)benzo[c]-[1,2,5]thiadiazole (**3**) and benzil (**5**) were used as reactants. Yield: 62% (light green solid). <sup>1</sup>H NMR (400 MHz, CDCl<sub>3</sub>):  $\delta$  (ppm) = 8.17 (s, 2H), 7.89 (d, 2H,  $J = 3.76$  Hz), 7.75 (m, 4H), 7.53 (d, 2H,  $J = 5.12$  Hz), 7.42-

7.38 (m, 6H), 7.20 (dd, 2H,  $J = 3.76, 5.12$  Hz).  $^{13}\text{C}$  NMR (100 MHz,  $\text{CDCl}_3$ ):  $\delta$  (ppm) = 154.3, 141.4, 141.3, 139.9, 133.9, 133.1, 131.7, 131.5, 130.9, 129.7, 129.3, 129.1. MALDI-TOF MS:  $m/z$  calcd, 446.586; found, 446.127 [ $\text{M}^+$ ].

## II-2.6. 2,3-Di(4-fluorophenyl)-5,8-di(thiophen-2-yl) quinoxaline (8)

Synthesis of compound **8** was followed by the general procedure for the acid-catalyzed reaction. 4,7-Di(thiophene-2-yl)benzo[*c*]-[1,2,5]thiadiazole (**3**) and 4,4'-difluorobenzil (**6**) were used as reactants. Yield: 58% (light green solid).  $^1\text{H}$  NMR (400 MHz,  $\text{CDCl}_3$ ):  $\delta$  (ppm) = 8.15 (s, 2H), 7.84 (d, 2H,  $J = 3.76$  Hz), 7.72 (dd, 4H,  $J = 5.36, 8.60$  Hz), 7.52 (d, 2H,  $J = 5.12$  Hz), 7.18 (dd, 2H,  $J = 5.12, 3.76$  Hz), 7.09 (t, 4H,  $J = 8.60$  Hz).  $^{13}\text{C}$  NMR (100 MHz,  $\text{CDCl}_3$ ):  $\delta$  (ppm) = 167.1, 165.2, 154.0, 153.0, 141.2, 139.8, 135.0, 131.6, 129.9, 129.3, 129.1, 118.2, 118.1, 110.0.  $^{19}\text{F}$  NMR (376 MHz,  $\text{CDCl}_3$ ):  $\delta$  (ppm) = -111.51. MALDI-TOF MS:  $m/z$  calcd, 482.567; found, 483.121 [ $\text{M}^+$ ].

### II-2.7. 6,7-Difluoro-2,3-diphenyl-5,8-di(thiophen-2-yl)quinoxaline (9)

Synthesis of compound **9** was followed by the general procedure for the acid-catalyzed reaction. 5,6-Difluoro-4,7-di(thiophen-2-yl)benzo[c][1,2,5]thiadiazole (**4**) and benzil (**5**) were used as reactants. Yield: 68% (yellow solid).  $^1\text{H}$  NMR (400 MHz,  $\text{CDCl}_3$ ):  $\delta$  (ppm) = 8.05 (d, 2H,  $J = 3.76$  Hz), 7.72 (m, 4H), 7.65 (d, 2H,  $J = 5.12$  Hz), 7.41-7.37 (m, 6H), 7.22 (dd, 2H,  $J = 3.76, 5.12$  Hz).  $^{13}\text{C}$  NMR (100 MHz,  $\text{CDCl}_3$ ):  $\delta$  (ppm) = 152.2, 138.8, 135.6, 131.6, 131.5, 131.4, 131.2, 130.8, 129.9, 129.0, 127.3  $^{19}\text{F}$  NMR (376 MHz,  $\text{CDCl}_3$ ):  $\delta$  (ppm) = -128.68. Mass,  $m/z$  calcd, 482.07; found, 481.85 [ $\text{M}^+$ ].

### II-2.8. 6,7-Difluoro-2,3-bis(4-fluorophenyl)-5,8-di(thiophen-2-yl)quinoxaline (10)

Synthesis of compound **10** was followed by the general procedure for the acid-catalyzed reaction. 5,6-Difluoro-4,7-di(thiophen-2-yl)benzo[c][1,2,5]thiadiazole (**4**) and 4,4'-difluorobenzil (**6**) were used as reactants. Yield: 65% (orange solid).  $^1\text{H}$  NMR (400 MHz,  $\text{CDCl}_3$ ):  $\delta$  (ppm) = 8.00 (d, 2H,  $J = 3.76$  Hz), 7.68 (dd, 4H,  $J = 5.36, 8.84$  Hz), 7.65 (d, 2H,  $J = 5.12$  Hz), 7.23 (dd, 2H,  $J = 3.76, 5.12$  Hz), 7.08 (t, 4H,  $J =$

8.84 Hz).  $^{13}\text{C}$  NMR (125 MHz,  $\text{CDCl}_3$ ):  $\delta$  (ppm) = 164.3, 162.6, 150.2, 134.7, 134.0, 132.4, 132.3, 130.9, 130.5, 130.1, 126.7, 117.9, 115.7, 115.5.  $^{19}\text{F}$  NMR (376 MHz,  $\text{CDCl}_3$ ):  $\delta$  (ppm) = -111.09, -128.18. Mass,  $m/z$  calcd, 518.55; found, 517.85 [ $\text{M}^+$ ].

### **II-2.9. General Procedure for Dibromination Reaction based on DPQ monomers**

A mixture of the appropriate DPQ compound (**7**, **8**, **9**, **10**; 1.0 mmol) and *N*-bromosuccinimide (NBS; 2.2 mmol) in THF (30 mL) was stirred at room temperature for 12 h. The reaction mixture was poured into water and extracted with ethyl acetate. The organic layers were separated, dried over magnesium sulfate and filtered. Solvents were removed under reduced pressure, and the crude residue was further purified by recrystallization from ethyl acetate/ethanol (1/4, v/v).

### **II-2.10. 5,8-Di(5-bromothiophen-2-yl)-2,3-diphenylquinoxaline (11)**

Synthesis of compound **11** was followed by the general procedure for the dibromination reaction. **7** was used as the starting material. Yield: 72% (orange solid).  $^1\text{H}$  NMR (400 MHz,  $\text{CDCl}_3$ ):  $\delta$  (ppm) = 8.12 (s, 2H), 7.71

(m, 4H), 7.59 (d, 2H,  $J = 2.68$  Hz), 7.44-7.40 (m, 6H), 7.14 (d, 2H,  $J = 2.68$  Hz).  $^{13}\text{C}$  NMR (100 MHz,  $\text{CDCl}_3$ ):  $\delta$  (ppm) = 154.8, 153.9, 142.2, 140.8, 139.2, 133.2, 133.1, 131.9, 130.9, 128.3, 128.2, 119.8. MALDI-TOF MS:  $m/z$  calcd, 604.378; found, 603.993 [ $\text{M}^+$ ].

### **II-2.11. 5,8-Di(5-bromothiophen-2-yl)-2,3-bis(4-fluorophenyl) quinoxaline (12)**

Synthesis of compound **12** was followed by the general procedure for the dibromination reaction. **8** was used as the starting material. Yield: 65% (light red solid).  $^1\text{H}$  NMR (400 MHz,  $\text{CDCl}_3$ ):  $\delta$  (ppm) = 8.09 (s, 2H), 7.68 (dd, 4H,  $J = 5.36, 8.88$  Hz), 7.55 (d, 2H,  $J = 4.32$  Hz), 7.13-7.09 (m, 6H).  $^{13}\text{C}$  NMR (100 MHz,  $\text{CDCl}_3$ ):  $\delta$  (ppm) = 167.0, 165.3, 153.5, 142.0, 139.2, 136.7, 135.0, 133.2, 131.8, 128.5, 119.9, 118.3, 118.2.  $^{19}\text{F}$  NMR (376 MHz,  $\text{CDCl}_3$ ):  $\delta$  (ppm) = -111.02. MALDI-TOF MS:  $m/z$  calcd, 640.359; found, 639.992 [ $\text{M}^+$ ].

### **II-2.12. 5,8-Di(5-bromothiophen-2-yl)-6,7-difluoro-2,3-diphenylquinoxaline (13)**

Synthesis of compound **13** was followed by the general procedure for the dibromination reaction. **9** was used as the starting material. Yield: 75% (orange solid).  $^1\text{H}$  NMR (400 MHz,  $\text{CDCl}_3$ ):  $\delta$  (ppm) = 7.76 (d, 2H,  $J$  = 4.28 Hz), 7.65 (m, 4H), 7.42-7.37 (m, 6H), 7.13 (d, 2H,  $J$  = 4.28 Hz).  $^{13}\text{C}$  NMR (100 MHz,  $\text{CDCl}_3$ ):  $\delta$  (ppm) = 152.6, 138.3, 135.1, 133.1, 131.8, 131.7, 131.6, 131.2, 130.1, 130.0, 129.1, 119.7.  $^{19}\text{F}$  NMR (376 MHz,  $\text{CDCl}_3$ ):  $\delta$  (ppm) = -128.36. Mass,  $m/z$  calcd, 640.36; found, 639.55 [ $\text{M}^+$ ].

### **II-2.13. 5,8-Di(5-bromothiophen-2-yl)-6,7-difluoro-2,3-bis(4-fluorophenyl)quinoxaline (14)**

Synthesis of compound **14** was followed by the general procedure for the dibromination reaction. **10** was used as the starting material. Yield: 70% (orange solid).  $^1\text{H}$  NMR (400 MHz,  $\text{CDCl}_3$ ):  $\delta$  (ppm) = 7.78 (d, 2H,  $J$  = 4.04 Hz), 7.64 (dd, 4H,  $J$  = 5.36, 8.84 Hz), 7.17 (d, 2H,  $J$  = 4.04 Hz), 7.11 (t, 4H,  $J$  = 8.60 Hz).  $^{13}\text{C}$  NMR (100 MHz,  $\text{CDCl}_3$ ):  $\delta$  (ppm) = 164.4, 162.8, 150.7, 134.2, 133.5, 132.4, 132.2, 131.2, 131.1, 129.5, 119.0, 115.8, 115.7.  $^{19}\text{F}$  NMR (376 MHz,  $\text{CDCl}_3$ ):  $\delta$  (ppm) = -110.59, -127.90. Mass,  $m/z$  calcd, 676.34; found, 675.60 [ $\text{M}^+$ ].

### **II-3. General Procedure for Polymerization by palladium-catalyzed Stille reaction**

In a Schlenk flask, BDT monomer (**15**, 0.25 mmol), dibrominated DPQ-based monomer (0.25 mmol) and Pd(PPh<sub>3</sub>)<sub>4</sub> (3 mol%) were dissolved in dry toluene (10 ml). After N<sub>2</sub> had been bubbled through for 15 min, the reaction mixture was heated to 90 °C and vigorously stirred for 2 d under a N<sub>2</sub> atmosphere and then 2-trimethylstannylthiophene and 2-bromothiophene were consecutively added as end-capping agents with an interval of 3 h. Once polymerization was complete, the mixture was cooled to room temperature and poured into methanol. The precipitated black solids were collected and further purified by Soxhlet extraction with methanol, acetone, hexane, and chloroform. The polymers in the chloroform fraction were recovered by precipitation into methanol again. Finally, the polymer was dried in a vacuum oven at 50 °C.

#### **II-3.1. Synthesis of PBDT-Qx**

Synthesis of polymer **PBDT-Qx** was followed by the general procedure for polymerization by palladium-catalyzed Stille reaction. **15** and **11** were used as reactants. Yield: 83% (deep purple solid). <sup>1</sup>H NMR (400 MHz, CDCl<sub>3</sub>): δ (ppm) = 8.02-7.72 (br, 8H), 7.65-7.36 (br, 6H), 7.24-

7.15 (br, 2H), 7.10-6.95 (br, 2H), 4.27-3.92 (br, 4H), 2.01-1.83 (br, 2H), 1.81-1.22 (br, 64H), 1.20-1.01 (br, 12H). Molecular weight by GPC: number-average molecular weight ( $M_n$ ) = 49.22 KDa, polydispersity index (PDI) = 2.64. Elemental analysis: calcd (%) for  $C_{78}H_{98}N_2O_2S_4$ : C 76.55, H 8.07, N 2.29, S 10.48; found: C 76.08, H 8.15, N 2.31, S 10.57.

### II-3.2. Synthesis of PBDT-QxF

Synthesis of polymer **PBDT-QxF** was followed by the general procedure for polymerization by palladium-catalyzed Stille reaction. **15** and **12** were used as reactants. Yield: 80% (deep purple solid).  $^1H$  NMR (400 MHz,  $CDCl_3$ ):  $\delta$  (ppm) = 8.12-7.65 (br, 10H), 7.48-7.32 (br, 2H), 7.23-7.01 (br, 4H), 4.27-3.95 (br, 4H), 2.01-1.83 (br, 2H), 1.81-1.22 (br, 64H), 1.20-1.01 (br, 12H). Molecular weight by GPC:  $M_n$  = 38.30 KDa, PDI = 3.01. Elemental analysis: calcd (%) for  $C_{78}H_{96}F_2N_2O_2S_4$ : C 74.36, H 7.68, N 2.22, S 10.18; found: C 74.16, H 7.84, N 2.16, S 10.23.

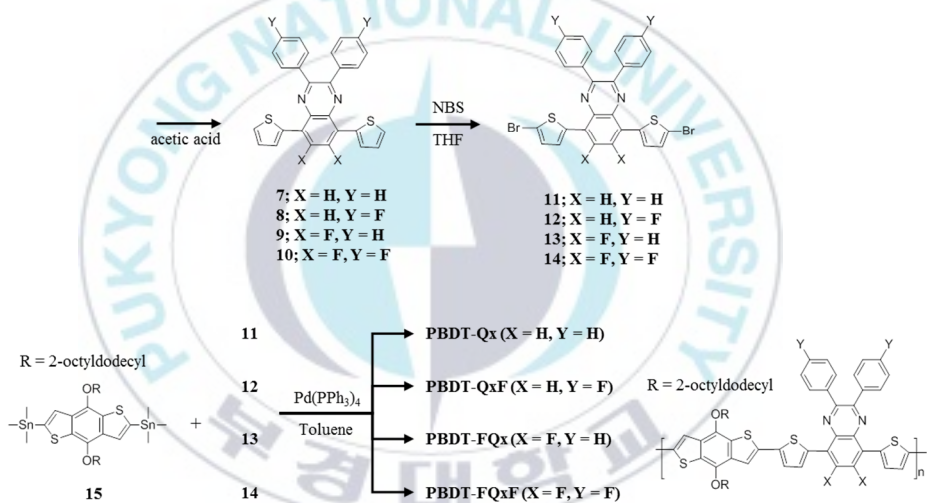
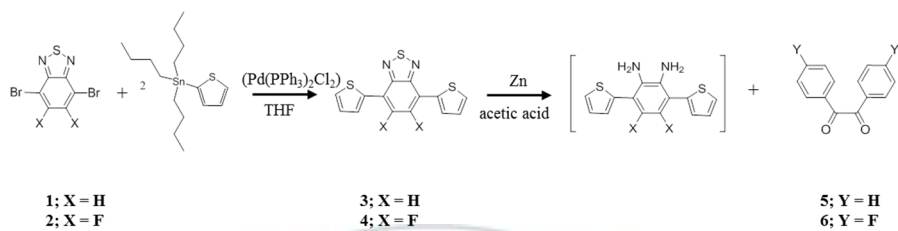
### II-3.3. Synthesis of PBDT-FQx

Synthesis of polymer **PBDT-FQx** was followed by the general procedure for polymerization by palladium-catalyzed Stille reaction. **15** and **13** were used as reactants. Yield: 85% (deep purple solid).  $^1H$  NMR

(400 MHz, CDCl<sub>3</sub>):  $\delta$  (ppm) = 8.21-7.85 (br, 4H), 7.82-7.41 (br, 8H), 7.21-7.01 (br, 4H), 4.27-3.95 (br, 4H), 2.01-1.83 (br, 2H), 1.81-1.22 (br, 64H), 1.20-1.01 (br, 12H). Molecular weight by GPC:  $M_n$  = 42.88 KDa, PDI = 2.53. Elemental analysis: calcd (%) for C<sub>78</sub>H<sub>96</sub>F<sub>2</sub>N<sub>2</sub>O<sub>2</sub>S<sub>4</sub>: C 74.36, H 7.68, N 2.22, S 10.18; found: C 74.11, H 7.81, N 2.24, S 10.22.

### II-3.4. Synthesis of PBDT-FQxF

Synthesis of polymer **PBDT-FQxF** was followed by the general procedure for polymerization by palladium-catalyzed Stille reaction. **15** and **14** were used as reactants. Yield: 78% (deep purple solid). <sup>1</sup>H NMR (400 MHz, CDCl<sub>3</sub>):  $\delta$  (ppm) = 8.22-7.61 (br, 6H), 7.49-7.31 (br, 2H), 7.22-7.05 (br, 6H), 4.27-3.95 (br, 4H), 2.01-1.83 (br, 2H), 1.81-1.22 (br, 64H), 1.20-1.01 (br, 12H). Molecular weight by GPC:  $M_n$  = 37.09 KDa, PDI = 3.24. Elemental analysis: calcd (%) for C<sub>78</sub>H<sub>94</sub>F<sub>4</sub>N<sub>2</sub>O<sub>2</sub>S<sub>4</sub>: C 72.30, H 7.31, N 2.16, S 9.90; found: C 71.91, H 7.50, N 2.24, S 10.23.



**Scheme 1.** Synthetic route of monomers and polymers

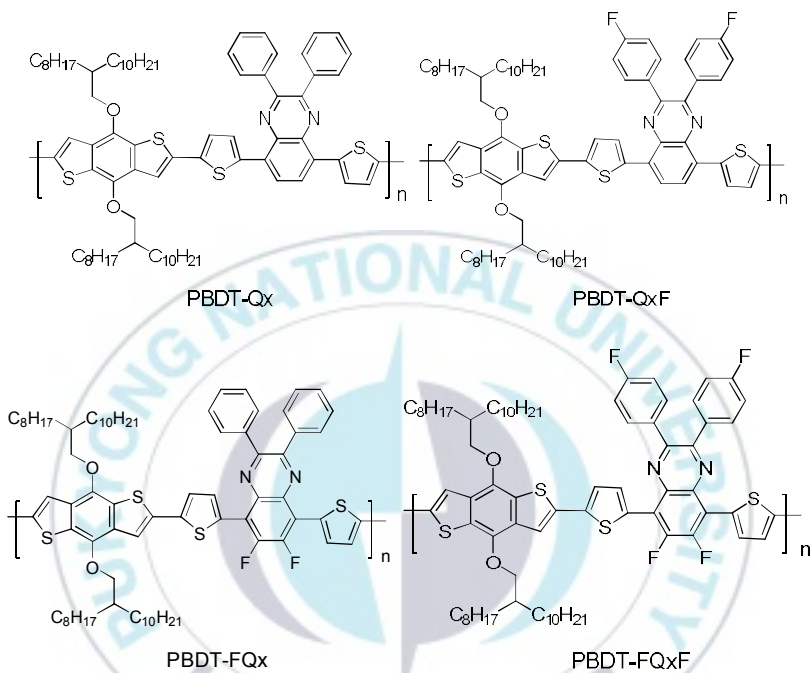


**Figure II-1.** Chemical structures of **PBDT-QxF**, **PBDT-QxF**, **PBDT-FQx**, and **PBDT-FQxF**

## II-4. Fabrication and analysis of photovoltaic devices

[6,6]-Phenyl C<sub>71</sub> butyric acid methyl ester (PC<sub>71</sub>BM, catalog no. nano-cPCBM-SF) was obtained from Nano-C, Inc. To fabricate inverted type PSCs with indium tin oxide (ITO)/ZnO/active layer (polymer:PC<sub>71</sub>BM)/MoO<sub>3</sub>/Ag, a 25-nm-thick ZnO film was initially deposited on an ITO surface by using a sol-gel process. The partially crystalline ZnO film was prepared by thermal curing of predeposited ZnO precursors at 200 °C for 10 min. The solution of ZnO precursors was prepared by the dissolution of zinc acetate dehydrate (0.164g) and ethanolamine (0.05 ml) in methoxyethanol (1mL) and stirring the mixture for 30 min prior to film deposition. The active layer with a thickness of 80 nm was fabricated using a chloroform solution of polymeric donor and PC<sub>71</sub>BM acceptor by spin-coating at 600 rpm for 60 s. Prior to spin-coating, the blended solution was filtered through a 0.2 μm polytetrafluoroethylene membrane filter. Finally, a 20-nm-thick MoO<sub>3</sub> layer and 100-nm-thick Ag layer were consecutively deposited by thermal evaporation at  $2 \times 10^{-6}$  Torr through a shadow mask with a device area of 0.13 cm<sup>2</sup>. The *J-V* characteristics of device were analyzed by using a KEITHLEY Model 2400 source-measure unit under AM 1.5G illumination at 100 mW/cm<sup>2</sup> from a 150 W Xe lamp. The conditions of

solar simulation were calibrated before the measurements by using a Si reference cell with a KG5 filter certified by the National Institute of Advanced Industrial Science and Technology.



## Chapter III. Results and Discussion

### III-1. Synthesis and Thermal Properties of Polymers

As shown in Scheme 1, compound **3** and **4** were synthesized by the Stille coupling reaction between compounds of **1**, **2** with 2-(tributylstannyl)thiophene, then continued by reduced with Zn powder to afford *ortho*-diamine intermediates and condensed with benzil (**5**) or 4,4'-difluorobenzil (**6**) to give the related DPQ compounds of **7**, **8**, **9**, and **10**. By this combination, four kinds of thiophene-containing DPQ derivatives with different positions and number of fluorine atoms in their chemical structure can be generated. Bromination of **7**, **8**, **9**, and **10** with N-bromosuccinimide (NBS) produce final monomers of dibrominated DPQ monomers of **11**, **12**, **13**, and **14**, respectively. Moreover, the electron-donating dialkoxy-substituted BDT monomer (**15**) was prepared to construct polymers with D- $\pi$ -A structures. In order to avoid solubility problems presumably caused by the DPQ-based comonomers without alkyl or alkoxy, a relative long alkyl of 2-octyldodecyloxy chains were incorporated into BDT monomer. The polymerization of **15** and DPQ-based co-monomer (**7**, **8**, **9**, and **10**) by Stille coupling reaction using Pd(PPh<sub>3</sub>)<sub>4</sub> as a catalyst successfully obtained **PBDT-Qx**, **PBDT-QxF**, **PBDT-FQx**, and **PBDT-FQxF**, respectively. The structures of all

synthesized compounds were confirmed by various analytical techniques. All polymers exhibit good solubility in common organic solvents such as chloroform, THF, and toluene. The number-average molecular weights ( $M_n$ ), weight-average molecular weights ( $M_w$ ) and the polydispersity index (PDI) of polymers were determined by using GPC measurements with THF as the eluent, exhibit a  $M_n$  relatively high were found in the range of 37.09 - 49.22 kDa with a PDI values of 2.53 – 3.01 (Table III-1).

**Table III-1.** Molecular weights of polymers

Polymer	$M_n$ (kDa)	$M_w$ (kDa)	PDI
PBDT-Qx	49.22	129.74	2.64
PBDT-QxF	38.30	115.45	3.01
PBDT-FQx	42.88	108.58	2.53
PBDT-FQxF	37.09	120.21	3.24

The thermal properties of polymers were evaluated by thermogravimetric analysis (TGA) at a heating rate of 10 °C/min under a  $N_2$  atmosphere as shown in Figure III-1. All the polymers presented a good thermal stability with a similar high onset of decomposition temperature with 5 wt % loss temperatures around 320 °C ( $T_{d5\%}$ ).

Moreover, differential scanning calorimetry (DSC) measurements of polymers in the temperature range from 25 to 250 °C showed no noticeable thermal transitions discovered during the cooling and heating processes (Figure III-2).

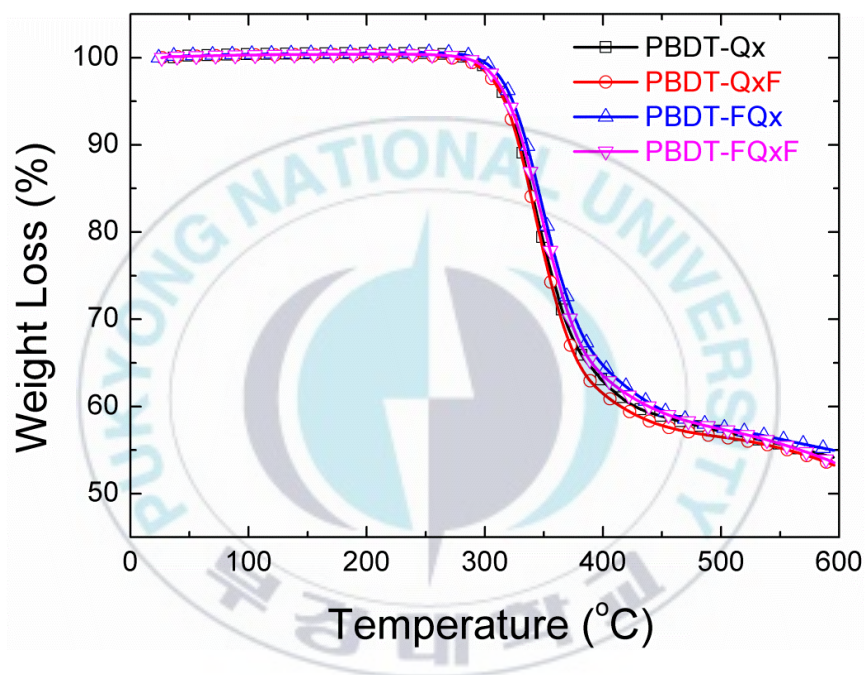


**Figure III-1.** TGA thermograms of **PBDT-Qx**, **PBDT-QxF**, **PBDT-FQx** and **PBDT-FQxF** at a heating rate of 10 °C/min under N<sub>2</sub>.

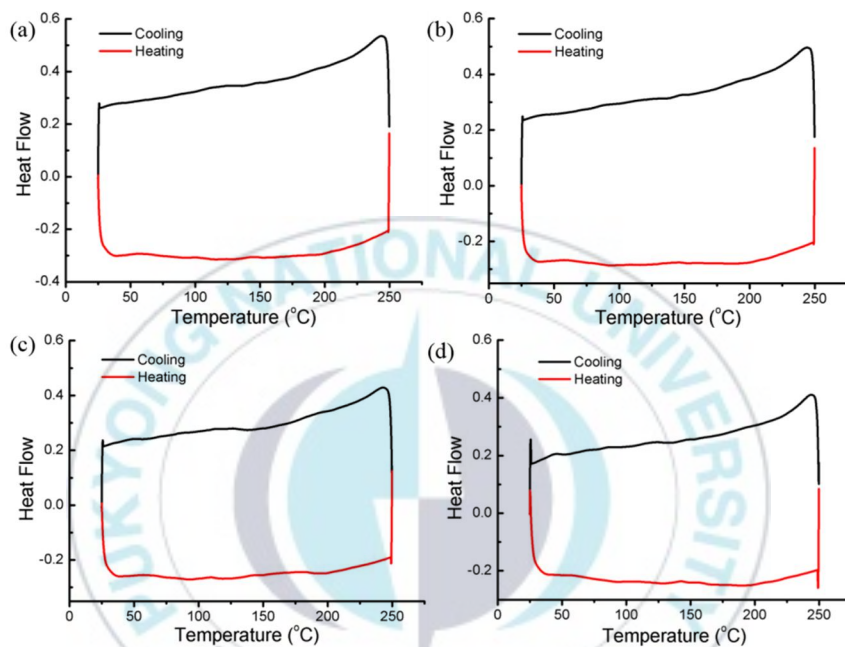


**Figure III-2.** First cooling and second heating DSC thermograms of polymers with cooling and heating rate of 10 °C/min under N<sub>2</sub>: (a) PBDT-QX; (b) PBDT-QxF; (c) PBDT-FQx; (d) PBDT-FQxF.

### III-2. Optical and Electrochemical Properties of Polymers

Optical properties of polymers were measured using UV-Vis spectra in chlorobenzene (CB) solution and solid thin film state as shown in Figure III-3a. All polymers exhibit two distinct absorption bands; a one at the shorter wavelength region (350-470 nm), originating from the localized  $\pi$ - $\pi^*$  transition of the polymers and a relatively broader one at longer wavelength region (500-750 nm) induced by a typical intramolecular charge-transfer (ICT), as exclusively observed in donor- $\pi$ -acceptor polymers. Compared to the absorption profiles in solutions, the positions of absorption bands of the polymer films are more red-shifted which is attributed of increased intermolecular interactions in the solid state. As summarized in Table III-2, the absorption maxima of the **PBDT-Qx**, **PBDT-QxF**, **PBDT-FQx**, and **PBDT-FQxF** film at ICT region are 624, 610, 611 and 611 nm, respectively. The optical band gaps ( $E_{gap}^{opt}$ ) of **PBDT-Qx**, **PBDT-QxF**, **PBDT-FQx**, and **PBDT-FQxF** which determined from the absorption edges are 1.67, 1.71, 1.73, and 1.73 eV, respectively. Furthermore the absorption maximum in the longer-wavelength region and the optical band gap are blue-shifted as an increase in the number of fluorine atoms on the DPQ unit. However, the absorption spectra of the polymer thin films of the fluorinated

quinoxaline-containing polymer **PBDT-Q<sub>x</sub>F**, **PBDT-FQ<sub>x</sub>**, and **PBDT-FQ<sub>x</sub>F** exhibit shoulders in the longer-wavelength region compared to non-fluorinated **PBDT-Q<sub>x</sub>**, which means substitution of fluorine atoms have visible influence on the photophysical properties of polymers by strong intermolecular or intramolecular aggregation through F-F and F-H interactions [29, 30, 31]. Herein, the blue-shifted absorption maximum is not seemed to be attributed from stronger ICT, but may due to the deeper HOMO after fluorination enlarge the band gap. The results agree well with previous reports [29, 32-35]. Moreover, the molar extinction coefficients ( $\epsilon$ ) (Fig. III-3b) at the absorption maximum wavelength of the polymer solutions with fluorine atoms are higher than that without fluorine atoms.

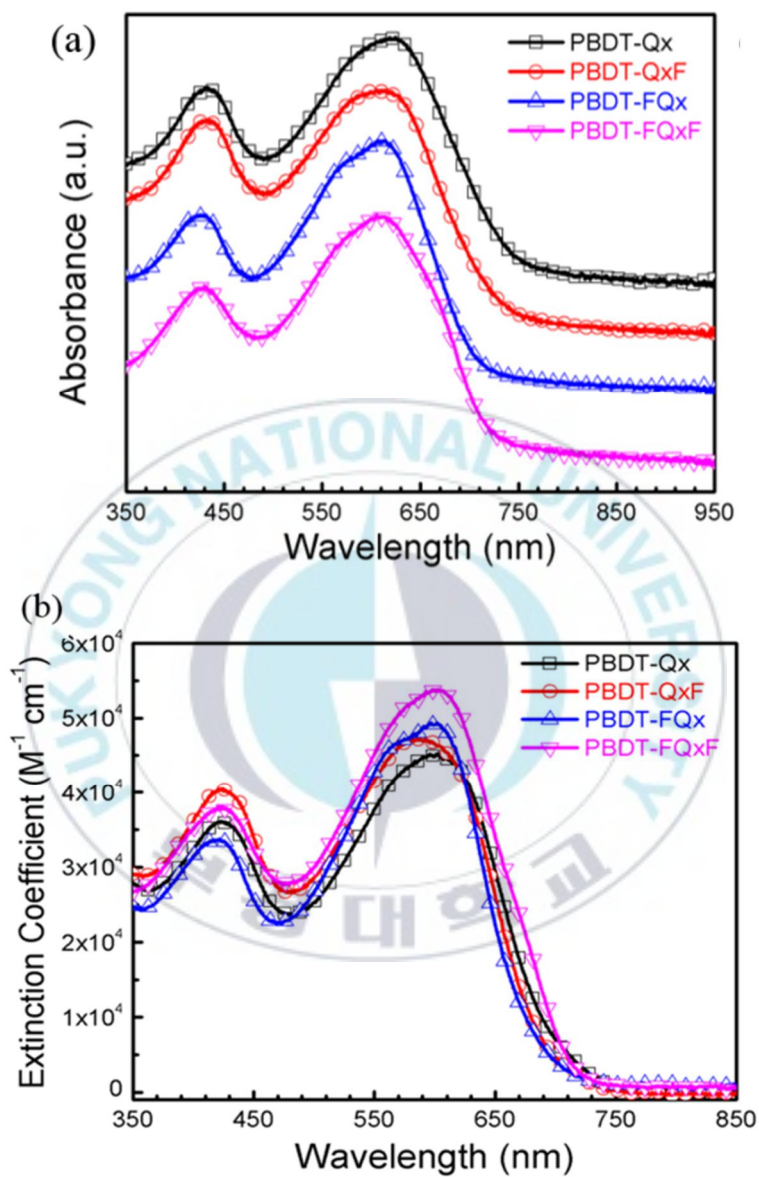


**Figure III-3.** (a) UV-visible spectra of polymer films on glass substrate (film spectra are offset for clarity) and (b) in chlorobenzene.

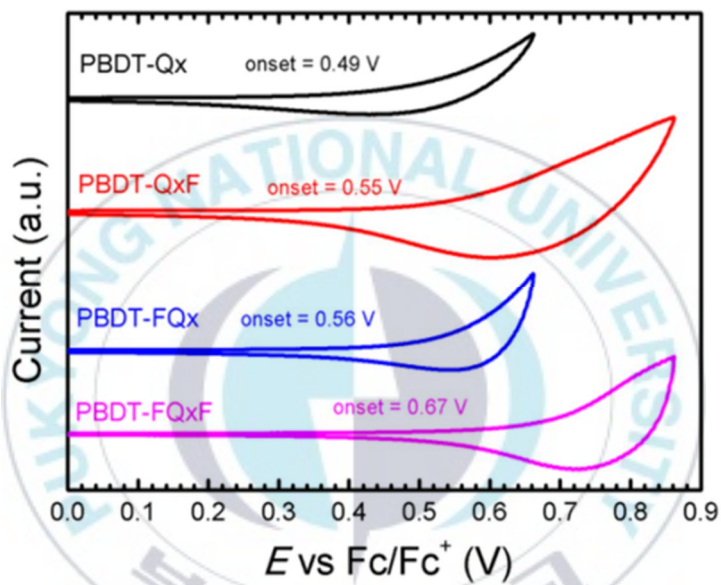


**Figure III-4.** Cyclic voltammograms of polymers.

**Table III-2.** Summary of optical and electrochemical properties of the polymers.

Polymers	$\lambda_{edge}$ (nm) <sup>a</sup> $E_{gap}^{opt}$ (eV) <sup>b</sup>	$\lambda_{max}^{film}$ (nm) <sup>c</sup>	HOMO (eV) <sup>d</sup>	LUMO (eV) <sup>e</sup>
PBDT-Qx	741 1.67	430, 624	- 5.29	- 3.62
PBDT-QxF	724 1.71	431, 610	- 5.35	- 3.64
PBDT-FQx	717 1.73	425, 611	- 5.36	- 3.63
PBDT- FQxF	718 1.73	426, 611	- 5.47	- 3.74

<sup>a</sup>Absorption edge of the film, <sup>b</sup>Estimated from the  $\lambda_{edge}$ , <sup>c</sup>Maximum wavelength of the film, <sup>d</sup>Estimated from the oxidation onset potential, <sup>e</sup>Calculated from the optical band gap and the HOMO energy level.

Figure III-4 shows cyclic voltammogram (CV) of the polymers have irreversible oxidation processes and the CV data are summarized in Table III-2. The HOMO energy levels of **PBDT-Q<sub>x</sub>**, **PBDT-Q<sub>x</sub>F**, **PBDT-FQ<sub>x</sub>**, and **PBDT-FQ<sub>x</sub>F** figured out from the oxidation onset potential are -5.29, -5.35, -5.36 and -5.47 eV, respectively. As increases number of substituted fluorine atoms, the HOMO levels become deeper due to the strong electronegativity of fluorine. The LUMO levels of **PBDT-Q<sub>x</sub>**, **PBDT-Q<sub>x</sub>F**, **PBDT-FQ<sub>x</sub>**, and **PBDT-FQ<sub>x</sub>F** were calculated using the HOMO energy levels and the optical band gap obtained from UV-visible absorption edges were -3.62, -3.64, -3.63, and -3.74 eV, respectively. The electronic energy level diagrams of the polymers, PC<sub>71</sub>BM, and other materials used for the fabrication of device were illustrated in Figure III-5. The LUMO and HOMO between the polymers and PC<sub>71</sub>BM should provide a sufficient driving force to guarantee efficient exciton dissociation at the D-A interface, which would ensure energetically favorable electron transfer [36].

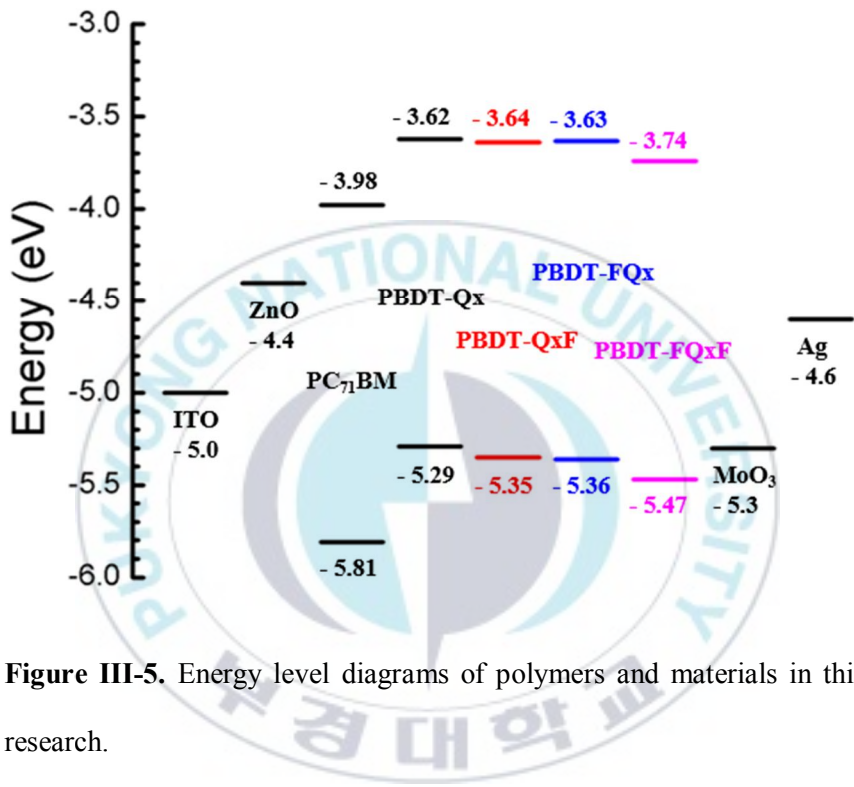
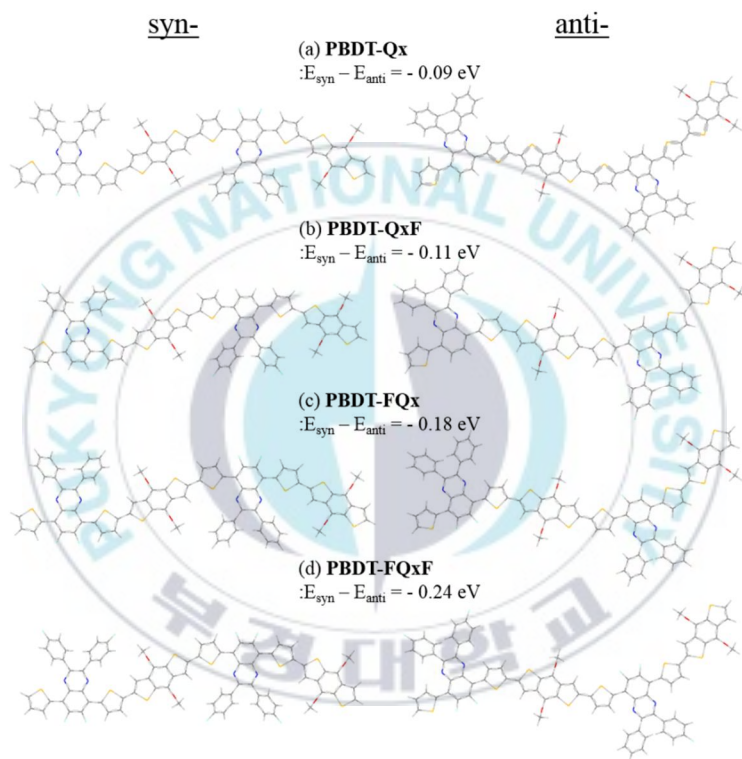


Figure III-5. Energy level diagrams of polymers and materials in this research.

### III-3. Theoretical Calculations of Polymers

To evaluate the fluorine effect by varying the number and position of F atoms and exploring the electronic structures of the DPQ-based low-band-gap polymers, the density functional theory (DFT) at the B3LP/6-31G\*\* level was carried out with the Gaussian 09 program. For simplicity, the 2-octyldodecyl side chains on the BDT unit and the long polymer backbones were replaced with methyl groups and two repeating units, respectively. To obtain optimized molecular geometries, conformational effects were thoroughly considered, due to there are two possible conformers with regard to the quinoxaline unit and adjacent thiophene linkers. One is a *syn*-conformer, i.e., the nitrogen atoms in quinoxaline and the sulfur atom in thiophene face on the same direction, and the other is an *anti*-conformer, i.e., the nitrogen atoms in quinoxaline and the sulfur atom in thiophene face opposite directions. The calculated potential energy differences between *syn*- and *anti*-conformers ( $E_{\text{syn}}-E_{\text{anti}}$ ) (Fig. III-6) for **PBDT-Qx**, **PBDT-QxF**, **PBDT-FQx**, and **PBDT-FQxF** are - 0.09, - 0.11, - 0.18, and - 0.24 eV, respectively. Therefore, the *syn*-conformation is more favored for all polymers, which agrees well with previous results [37]. The frontier molecular orbitals of the two repeating units with theoretical HOMO/LUMO energy levels are shown in Figure

III-7. Overall, the calculated HOMO/LUMO energy levels exhibit similar trends to those observed in the UV-vis and CV experiments.



**Figure III-6.** Optimized geometries of the two repeating unit models of the DPQ-based polymers with a syn- and anti- configuration obtained by DFT calculation.

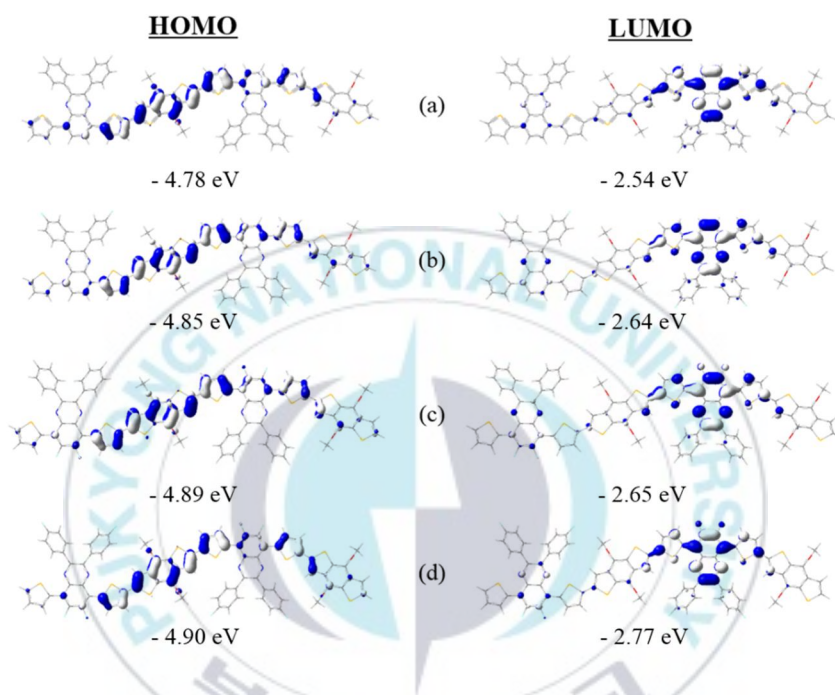


**Figure III-7.** Frontier molecular orbitals of two-repeating unit models with HOMO/LUMO energy levels calculated at the B3LYP/6-31G\*\* level for (a) **PBDT-Q<sub>x</sub>**, (b) **PBDT-Q<sub>x</sub>F**, (c) **PBDT-FQ<sub>x</sub>**, and (d) **PBDT-FQ<sub>x</sub>F**.

### III-4. Photovoltaic Properties of Polymers

In order to investigate the impact of fluorination, BHJ PSCs were fabricated with a device structure of ITO/ZnO (25 nm)/polymer:PC<sub>71</sub>BM (80 nm)/MoO<sub>3</sub> (10 nm)/Ag (100 nm). The active layers of these devices were spin-coated from o-dichlorobenzene (o-DCB) solutions. PSCs based on **PBDT-Qx** and **PBDT-QxF** with different blend ratios of polymers and PC<sub>71</sub>BM varied from 3:1 to 3:9 (w/w) have been fabricated and tested to optimize the device fabrication conditions. The optimized blend ratios were found to be 3:3 (polymer: PC<sub>71</sub>BM) with 1,8-diodooctane (DIO) as a processing additive. Figure III-8a shows current density-voltage (*J-V*) curves of photovoltaic devices based on polymers at the optimized blend ratio under AM 1.5G simulated illumination, and the corresponding short-circuit currents ( $J_{sc}$ ), open-circuit voltages ( $V_{oc}$ ), fill factors (*FF*) and power conversion efficiencies (PCE) are listed in Table III-3.

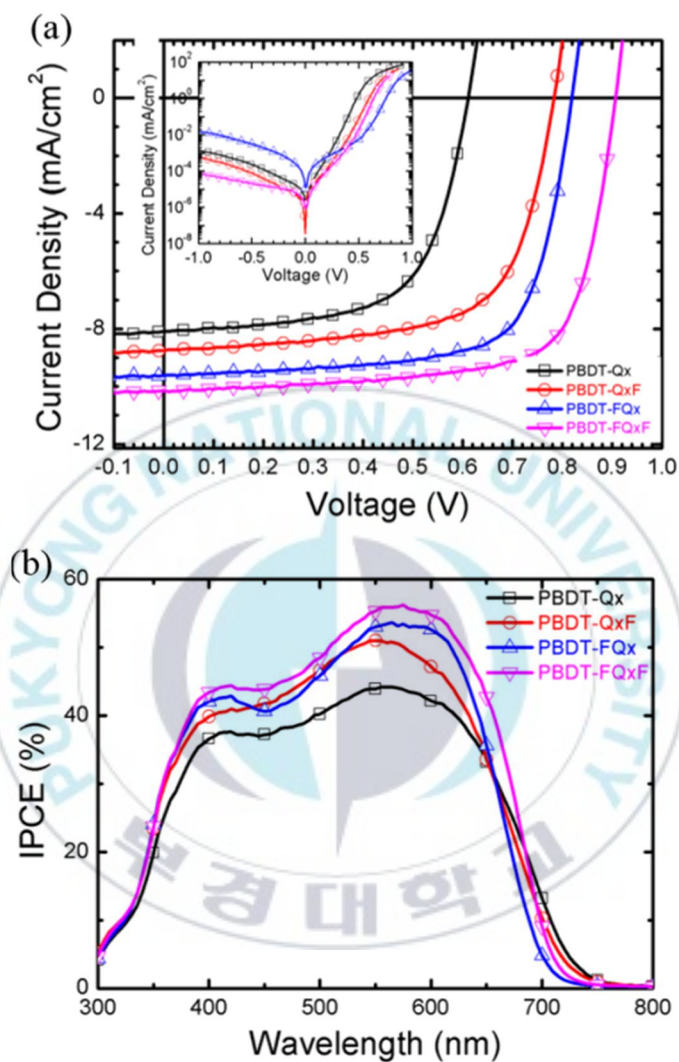


**Figure III-8.** (a) Current density vs. voltage curves of PSCs under 1.0 sun condition (inset: under the dark condition) and (b) IPCE spectra of PSCs based on **PBDT-Qx** (square), **PBDT-QxF** (circle), **PBDT-FQx** (triangle) and **PBDT-FQxF** (inverted triangle).

**Table III-3.** The best photovoltaic parameters of the PSCs. The averages for the photovoltaic parameters of each device are given in parentheses.

	$J_{sc}$ (mA/cm <sup>2</sup> )	$V_{oc}$ (V)	$FF$ (%)	$PCE$ (%)	$R_s$ ( $\Omega$ cm <sup>2</sup> ) <sup>a</sup>
	8.08	0.61	63.7	3.14	
<b>PBDT-Qx</b>	(7.87 ± 0.19)	(0.61 ± 0.00)	(63.1 ± 0.5)	(3.05 ± 0.07)	4.02
<b>PBDT- QxF</b>	8.76 (8.57 ± 0.11)	0.78 (0.78 ± 0.00)	66.1 (66.0 ± 0.1)	4.52 (4.42 ± 0.06)	3.60
<b>PBDT- FQx</b>	9.62 (9.49 ± 0.13)	0.82 (0.82 ± 0.00)	70.5 (70.2 ± 0.3)	5.56 (5.46 ± 0.08)	2.59
<b>PBDT- FQxF</b>	10.15 (9.97 ± 0.09)	0.91 (0.91 ± 0.00)	71.5 (71.6 ± 0.4)	6.60 (6.49 ± 0.07)	2.27

<sup>a</sup>Series resistance estimated from the corresponding best device.

The devices based on the polymers with fluorine substituents, **PBDT-QxF**, **PBDT-FQx**, and **PBDT-FQxF** showed a gradual enhancement PCEs of 4.52%, 5.56%, and 6.60%, respectively, which are significantly higher than that of the standard, non-fluorinated **PBDT-Qx** (3.14%). The

$V_{oc}$  values of the devices fabricated with **PBDT-QxF**, **PBDT-FQx**, and **PBDT-FQxF** are 0.78, 0.82, and 0.91 V, respectively, which show 27.9%, 34.4%, and 49.2% increase relative to the device based on **PBDT-Qx** (0.61 V). Due to introducing fluorine atoms in varied position and varied numbers in chemical structure of polymers, the HOMO energy levels became lower which lead to the higher  $V_{oc}$ . The  $J_{sc}$  data of the devices based on **PBDT-QxF**, **PBDT-FQx**, and **PBDT-FQxF** are -8.76, -9.62, and -10.15 mA/cm<sup>2</sup>, respectively, which also indicate 8.4%, 19.1%, and 25.6% increases compared with that of the **PBDT-Qx** based device (-8.08 mA/cm<sup>2</sup>). The change of the  $J_{sc}$  data of the devices under 1.0 sun illumination showed very good agreement with the incident photon-to-current efficiency (IPCE; Figure 8b) curves. The IPCE data at 400-700 nm of the devices based on the polymers of **PBDT-QxF**, **PBDT-FQx**, and **PBDT-FQxF** are higher than that of the device fabricated with **PBDT-Qx**. The series resistance ( $R_s$ ) data were obtained from the inverse slope at high current regime of  $J$ - $V$  curves in the dark (inset of Figure 8a). As shown in Table III-3, the  $R_s$  data showed smaller values upon an increase in the number of fluorine atoms and agreed well with the  $J_{sc}$  and  $FF$  values.

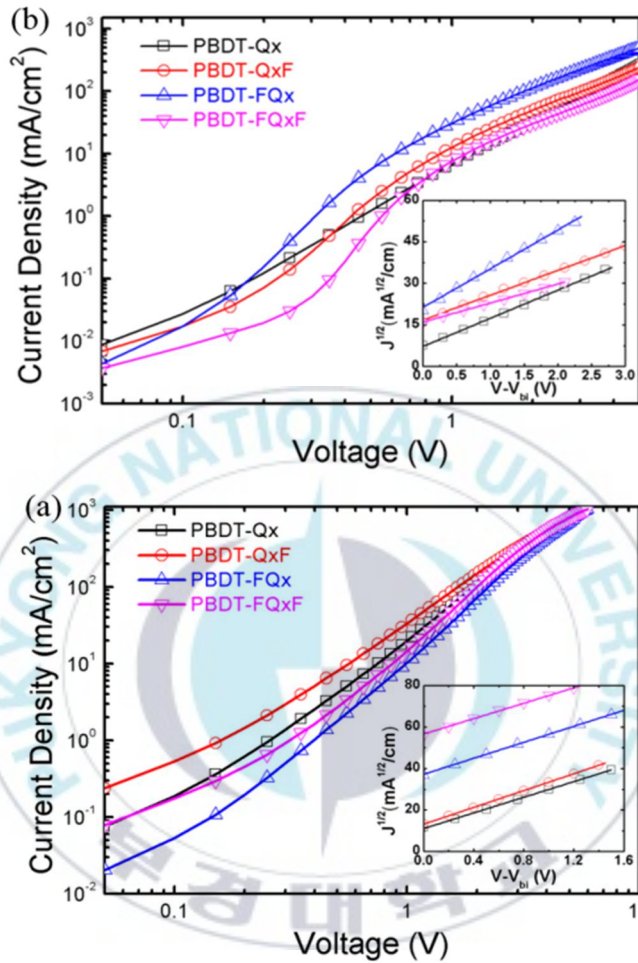


**Figure III-9.** Current density vs. voltage curves of (a) electron- and (b) hole-only devices (inset: current density vs. voltage - built-in voltage ( $V_{bi}$ ) curves with fitted lines) based on **PBDT-Qx** (square), **PBDT-QxF** (circle), **PBDT-FQx** (triangle) and **PBDT-FQxF** (inverted triangle).

To investigate charge transporting properties through the space charge limited current (SCLC) methods, electron- and hole- only devices with a structure of ITO/PEDOT:PSS (35 nm)/polymer:PC<sub>71</sub>BM (ca. 90 nm)/Au (50 nm) and ITO/ZnO (25 nm)/polymer:PC<sub>71</sub>BM (ca. 90 nm)/Al (100 nm), respectively, have been fabricated and tested. As shown in Figure III-9a and b, the  $J$ - $V$  curves showed a characteristic of SCLC. This can be expressed using the Mott-Gurney law [38];

$$J = \frac{9}{8} \epsilon_0 \epsilon_r \mu \frac{E^2}{L}$$

Which  $J$  is the current density,  $\epsilon_0 \epsilon_r$  is the permittivity of the active layer,  $\mu$  is the charge mobility,  $E$  is the electric field, and  $L$  is the thickness of the active layer. The electron mobilities of the device with **PBDT-Qx**, **PBDT-QxF**, **PBDT-FQx**, and **PBDT-FQxF** are  $2.5 \times 10^{-3}$ ,  $2.9 \times 10^{-3} \text{ s}^{-1}$ ,  $2.6 \times 10^{-3}$  and  $2.4 \times 10^{-3} \text{ cm}^2\text{V}^{-1}\text{s}^{-1}$ , respectively. The electron mobilities of the polymers with or without fluorine atoms are almost similar. The hole mobilities of the devices **PBDT-Qx**, **PBDT-QxF**, **PBDT-FQx**, and **PBDT-FQxF**, showed increased value of  $6.95 \times 10^{-4}$ ,  $8.67 \times 10^{-4}$ ,  $9.83 \times 10^{-4}$ , and  $9.86 \times 10^{-4} \text{ cm}^2\text{V}^{-1}\text{s}^{-1}$ , respectively. However, the ratios of hole to electron mobilities of the polymers with fluorine atoms are higher than that of the device based on **PBDT-Qx**,

and the highest value for **PBDT-FQxF** is demonstrated. The ratio is used to understand the optoelectronic properties of BHJ, particularly with respect to the  $J_{sc}$  and the  $FF$  values. SCLC results displayed the reason devices based on fluorine-substituted polymers have better photovoltaic properties.

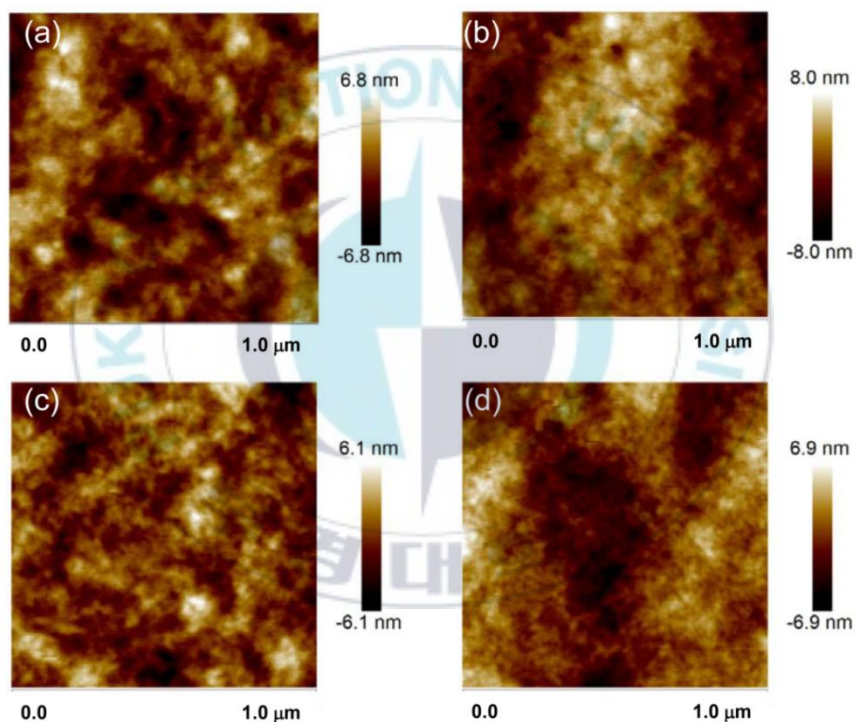
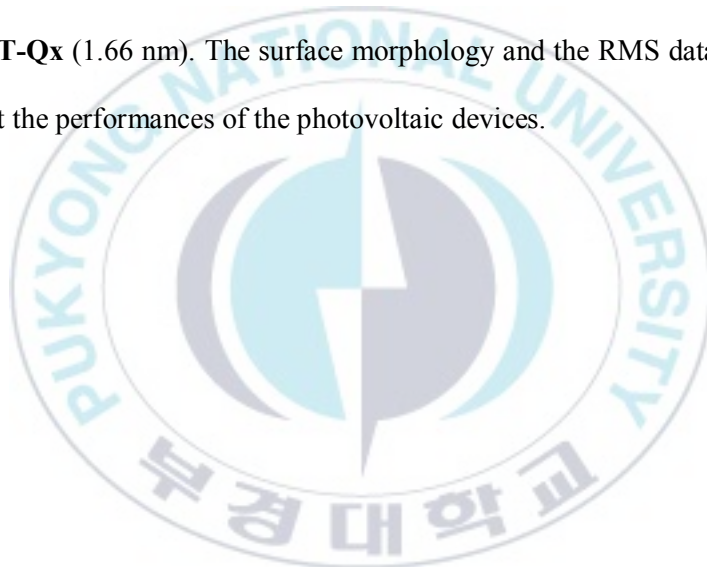


**Figure III-10.** AFM images of the active layers based on (a) **PBDT-Qx**, (b) **PBDT-QxF**, (c) **PBDT-FQx**, and (d) **PBDT-FQxF**.

The morphology of the active layers investigated by tapping-mode atomic force microscopy (AFM) measurements (Figure III-10). The root-mean-squares (RMSs) of the surface of the active layers based on **PBDT-QxF**, **PBDT-FQx**, and **PBDT-FQxF** are 2.04, 1.35, 1.67 nm, respectively, which values are almost identical to that of the surface of **PBDT-Qx** (1.66 nm). The surface morphology and the RMS data hardly affect the performances of the photovoltaic devices.



## Chapter IV. Conclusion

In summary, we have designed and synthesized a series of fluorinated quinoxaline-based polymers via Stille coupling reaction. The four polymers were composed by electron-donating dialkoxy-substituted BDT moiety and the electron-withdrawing DPQ unit which connected through a thiophene bridge to generate donor- $\pi$ -acceptor type PSCs. In order to investigate the effect of strong electron withdrawing F atoms, the DPQ units were substituted by F atoms in various numbers and at diver positions. As a result, optical and electrochemical showed the significant impact of fluorination in the electronic properties of polymers. In particular, the PCEs were gradually enhanced as increasing the number and positions of F substituents on the DPQ unit of polymers compared to non-fluorinated PBDT-Qx (3.14%), were 4.52%, 5.56%, and 6.60% of PBDT-QxF, PBDT-FQx, and PBDT-FQxF, respectively. Furthermore, more balanced electron-hole mobility with smaller series resistance has been obtained. This study can clearly represent favorable contributions of F atoms in quinoxaline-based conjugated polymers as one of promising approaches to improving the photovoltaic performance of PSCs.

## References

- [1] L. Lu, T. Zheng, Q. Wu, A.M. Schneider, D. Zhao, L. Yu, *Chem. Rev.* 115, 12666 (2015).
- [2] J. You, L. Dou, K. Yoshimura, T. Kato, K. Ohya, T. Moriarty, K. Emery, C.-C. Chen, J. Gao, G. Li, Y. Yang, *Nat. Commun.* 4, 1446 (2013).
- [3] B. Kan, Q. Zhang, M. Li, X. Wan, W. Ni, G. Long, Y. Wang, X. Yang, H. Feng, Y. Chen, *J. Am. Chem. Soc.* 136, 15529 (2014).
- [4] Z. He, B. Xiao, F. Liu, H. Wu, Y. Yang, S. Xiao, C. Wang, T. P. Russell, Y. Cao, *Nat. Photonics* 9, 174 (2015).
- [5] Y.-J. Cheng, S.-H. Yang, C.-S. Hsu, *Chem. Rev.* 109, 5868 (2009).
- [6] R.C. Chiechi, R.W.A. Havenith, J.C. Hummelen, L.J.A. Koster, M.A. Loi, *Materials Today* 16, 281 (2013).
- [7] H. Bässler and A. Köhler, *Top. Curr. Chem.*, 312, 1 (2012).
- [8] X.Y. Zhu, Q. Yang, and M. Muntwiler, *Acc. Chem. Res.* 42, 1779 (2009).
- [9] G.A.H. Wetzelaer and P.W.M. Blom, *NPG Asia Mater.* 6, e110 (2014).

- [10] G. Yu, J. Gao, J.C. Hummelen, F. Wudl, A.J. Heeger, *Science* 270, 1789 (1995).
- [11] X.-P. Xu, Y. Li, M.-M. Luo, Q. Peng, *Chin. Chem. Lett.* 27, 1241 (2016).
- [12] G. Dennler, M.C. Scharber, C.J. Brabec, *Adv. Mater.* 21, 1323 (2009).
- [13] H.Y. Chen, J.H. Hou, S.Q. Zhang, *Nat. Photonics* 3, 649 (2009).
- [14] Y. Li, *Acc. Chem. Res.* 45, 723 (2012).
- [15] H.X. Zhou, L.Q. Yang, A.C. Stuart, *Angew. Chem. Int. Ed.* 50, 2995 (2011).
- [16] B.C. Schroeder, Z.G. Huang, R.S. Ashraf, *Adv. Funct. Mater.* 22, 1663 (2012).
- [17] T.L. Nguyen, H. Choi, S.J. Ko, *Energy Environ. Sci.* 7, 3040 (2014).
- [18] C.H. Duan, A. Furlan, J.J. Van Franeker, *Adv. Mater.*, 27, 4461 (2015).
- [19] Q. Peng, X.J. Liu, D. Su, *Adv. Mater.* 23, 4554 (2011).
- [20] A.C. Stuart, J.R. Tumbleston, H.X. Zhou, *J. Am. Chem. Soc.* 135, 1806 (2013).

- [21] N. Wang, Z. Chen, W. Wei, Z.H. Jiang, *J. Am. Chem. Soc.* 135, 17060 (2013).
- [22] S. Albrecht, S. Janietz, W. Schindler, *J. Am. Chem. Soc.* 134, 14932 (2012).
- [23] C. Liu, K. Wang, X. Gong, and A.J. Heeger, *Chem. Soc. Rev.* 45, 4825 (2016).
- [24] V.A. Mamedov and N.A. Zhukova, ed. G.W. Gribble and J.A. Joule, Elsevier, Amsterdam, vol. 25, pp. 1–45 (2013).
- [25] D.W. Chang, H.J. Lee, J.H. Kim, S.Y. Park, S.-M. Park, L. Dai, and J.-B. Baek, *Org. Lett.* 13, 3880 (2011).
- [26] D. Kitazawa, N. Watanabe, S. Yamamoto, J. Tsukamoto, *Sol. Energy Mater. Sol. Cells* 98, 203 (2012).
- [27] J. Yuan, J. Ouyang, V. Cimrova, M. Leclerc, A. Najari and Y. Zou, *J. Mater. Chem. C* 5, 1858 (2017).
- [28] K.W. Song, T.H. Lee, E.J. Ko, K.H. Back, D.K. Moon, *J. Polym. Sci. Part A: Polym. Chem.* 52, 1028 (2014).
- [29] S.K. Putri, M.S. Lee, D.W. Chang, J.H. Kim, *Synth. Met.* 220, 455 (2016).
- [30] Q. Fan, Y. Liu, P. Yang, W. Su, M. Xiao, J. Chen, M. Li, X. Wang, Y. Wang, H. Tan, R. Yang, W. Zhu, *Org. Electron.* 23, 124 (2015).

- [31] D. Dang, W. Chen, R. Yang, W. Zhu, W. Mammod, E. Wang, *Chem. Commun.* 49, 9335 (2013).
- [32] S.C. Price, A.C. Stuart, L. Yang, H. Zhou, W. You, *J. Am. Chem. Soc.* 133, 4625 (2011).
- [33] Y. Liang, D. Feng, Y. Wu, S.-T. Tsai, G. Li, C. Ray, L. Yu, *J. Am. Chem. Soc.* 131, 7792 (2009).
- [34] H. Zhou, L. Yang, A.C. Stuart, S.C. Price, S. Liu, W. You, *Angew. Chem. Int. Ed.* 123, 3051 (2011).
- [35] F. Wu, Z. Deng, C. Li, L. Chen, Y. Chen, *J. Phys. Chem. C* 119, 8038 (2015).
- [36] C.J. Brabec, C. Winder, N.S. Sariciftci, J.C. Hummelen, A. Dhanabalan, P.A. Van Hal and R.A.J. Janssen, *Adv. Funct. Mater.* 12, 709 (2002).
- [37] D. Gedefaw, M. Tassarolo, W. Zhuang, R. Kroon, E. Wang, M. Bolognesi, M. Seri, M. Muccini, M.R. Andersson, *Polym. Chem.* 5, 2083 (2014).
- [38] A. Bagui, S.S.K. Iyer, *Org. Electron.* 15, 1387 (2014).

## **Acknowledgements**

I would like to express my deepest thanks during my master studies:

To Jesus Christ, the center of my life, for His tremendous blessing, to be my shield, my strength and my power to lighting every paths in my life

To my great supervisor, Professor Dong Wook Chang, for all amazing lessons he bring to my life and for his concern that motivated me to be a great person, I am very grateful and the lucky one to join in Functional Polymer Laboratory

To my second supervisor, Professor Joo Hyun Kim, for his advices during research work. Also to all professor in Department of Industrial Chemistry: Min Young Shon, Youngeup Jin, Ji Hwan Park and all officers who always help me

To my labmates sonbae minseok, oppa uk, honghye, miss song, munho, junte and shinta, to all teamwork and hard work I learn from

To my colleagues, pak otje, pak dagus, kak devi, bang david, mutia, mba moli, nadhila, ci lisa, mba nurul, mba listi, ci hana, nico, koh nico, vani, sony, limpat, siti, zeno, mba sabrina for all laughs and jokes we did last two years

To bapak nanang and ibu ester, to be my parents during I stayed in Korea and so on, and Sooyoungro Indonesia Church family with all kindhearted chipsanim, for all memories, sharing and caring that make my life in Korea more beautiful and feels like home

To my all lifetime friends, dinvax, alviano, tongki, elisa, salathiella, asri, mitha, yohana, lala for never ending friendship

To my abang david and his families, om and tante, for all loves, prays and supports, for inspiring me to be a better person

To my dearest mom for her great patiences and be my big motivation for pursue my studies, my sis nathalia and my bro robby, om anton fam and om joko fam, my unlimited loves, my whole family, this thesis I presented for you

Pukyong National University, Busan, South Korea

August 2017

Sella Kurnia Putri